Petrography and geochemistry of the Ngaoundéré Pan-African granitoids in Central North Cameroon: Implications for their sources and geological setting.

Rigobert Tchameni, André Pouclet, J. Penaye, A.A. Ganwa, S.F. Toteu

Petrography and geochemistry of the Ngaoundéré Pan-African granitoids in Central North Cameroon: Implications for their sources and geological setting

R. Tchameni[a], A. Pouclet[b], J. Penaye[c], A.A. Ganwa[a] and S.F. Toteu[c]

[a]Département des Sciences de la Terre, Faculté des Sciences, Université de Ngaoundéré, B.P. 454, Ngaoundéré, Cameroon
[b]Institut des Sciences de la Terre, UMR 6113, Université d'Orléans, B.P. 6759, 45067 Orléans cedex 2, France
[c]Centre for Geological and Mining research (CRGM), B.P. 333 Garoua, Cameroon

Keywords: Central North Cameroon; Pan-African granitoids; Geochemistry; Th–U–Pb monazite age

Abstract

The Nagoundéré Pan-African granitoids in Central North Cameroon belong to a regional-scale massif, which is referred to as the Adamawa-Yade batholith. The granites were emplaced into a ca. 2.1 Ga remobilised basement composed of metasedimentary and meta-igneous rocks that later underwent medium- to high-grade Pan-African metamorphism. The granitoids comprise three groups: the hornblende–biotite granitoids (HBGs), the biotite ± muscovite granitoids (BMGs), and the biotite granitoids (BGs). New Th–U–Pb monazite data on the BMGs and BGs confirm their late Neoproterozoic emplacement age (ca. 615 ± 27 Ma for the BMGs and ca. 575 Ma for the BGs) during the time interval of the regional tectono-metamorphic event in North Cameroon. The BMGs also show the presence of ca. 926 Ma inheritances, suggesting an early Neoproterozoic component in their protolith.

The HBGs are characterized by high Ba–Sr, and low K_2O/Na_2O ratios. They show fairly fractionated REE patterns (La_N/Yb_N 6–22) with no Eu anomalies. The BMGs are characterized by higher K_2O/Na_2O and Rb/Sr ratios. They are more REE-fractionated (La_N/Yb_N = 17–168) with strong negative Eu anomalies (Eu/Eu^* = 0.2–0.5). The BGs are characterized by high SiO_2 with $K_2O/Na_2O > 1$. They show moderated fractionated REE patterns (La_N/Yb_N = 11–37) with strong Eu negative anomalies (Eu/Eu^* = 0.2–0.8) and flat HREE features (Gd_N/Yb_N = 1.5–2.2). In Primitive Mantle-normalized multi-element diagrams, the patterns of all rocks show enrichment in LILE relative to HFSE and display negative Nb–Ta and Ti anomalies. All the granitoids belong to high-K calc-alkaline suites and have an I-type signature.

Major and trace element data of the HBGs are consistent with differentiation of a mafic magma from an enriched subcontinental lithospheric mantle, with possible crustal assimilation. In contrast, the high Th content, the LREE-enrichment, and the presence of inherited monazite suggest that the BGs and BMGs were derived from melting of the middle continental crust. Structural and petrochemical data indicate that these granitoids were emplaced in both syn- to post-collision tectonic settings.

1. Introduction

The Central African Fold belt (CAFB) in Cameroon is dominated in its central part by abundant late-Pan-African granitoids (Fig. 1), which extend south of the Tchollire-Banyo shear zone up to the Bertoua region and continue eastward into the Yade massif (Central African Republic and Chad). The granitoids belong to a complex batholith referred to here as the Adamawa-Yade batholith. The importance of this batholith results from its location north of the late-Neoproterozoic nappe system of southern Cameroon and its emplacement into a remobilised Paleoproterozoic basement that is interpreted as part of an active continental margin (Toteu et al., 2001 and Toteu et al., 2004). The importance of the Adamawa-Yade batholith also results from its spatially close association with major transcurrent shear zones of central Cameroon (Dumont, 1986, Ngako et al., 1991 and Ngako et al., 2003). These shear zones continue into NE Brazil, where they control the emplacement of late-Brasiliano (Pan-African) granitoids (Neves et al., 1996, Neves et al., 2000, Guimarães and da Silva Filho, 2000 and Guimarães et al., 2004).

Despite this importance, the Adamawa-Yadé batholith is poorly surveyed, particularly with regard to geochemical and geochronological studies. Data exist only for a few isolated massifs, which probably belong to another batholith in south-western Cameroon (Tagne-Kamga et al., 1999, Tagne-Kamga, 2003, Nguiessi Tchankam et al., 1997 and Nzolang et al., 2003). In this paper, we report petrographical, geochemical and geochronological data on the Ngaoundéré granitoids, which permit discussion of the source and tectonic setting of the Adamawa-Yade batholith.

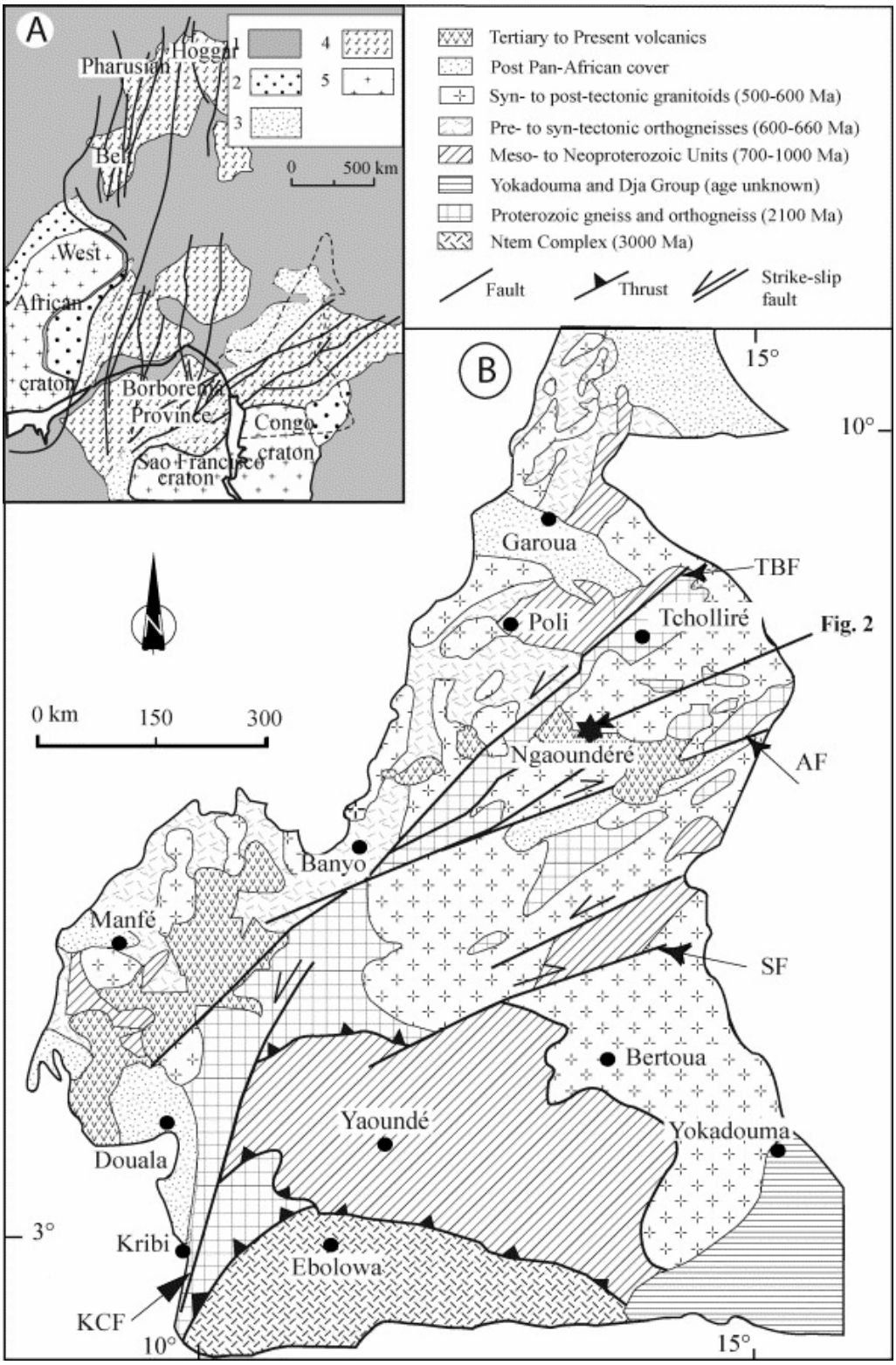

Fig. 1. Geological context (A) Geology of West-central Africa and northern Brazil in a Gondwana (pre-drift) reconstruction (modified from Castaing et al., 1994 and Toteu et al., 2001). Dashed line boundary of Cameroon. Thick line, boundary of the two continents: (1) Phanerozoic cover; (2) Neoproterozoic formations; (3) Regions of Brasiliano/Pan-African deformation in which Paleoproterozoic basement is absent or only present as small isolated blocks; (4) Regions of Brasiliano/Pan-African deformation with large amounts of reworked Paleoproterozoic basement; (5) cratons; (6) faults. (B) Simplified geological map of Cameroon (after Toteu et al., 2001) showing the location of the Ngaoundéré plutonic and major lithotectonic units. KCF, Kribi-Campo fault; AF, Adamaoua fault; SF, Sanaga fault; TBF, Tcholliré-Banyo fault.

2. Regional geological setting

The Adamawa-Yade massif is dominated by a NE–SW elongated regional-scale plutonic complex intrusive into a Paleoproterozoic basement and locally covered by Cretaceous deposits (Mbere and Koum basins) and by Cainozoic volcanic rocks of the Cameroon line. The hosting basement rocks, which now crop out as large septa within the batholith, comprise 2.1 Ga high-grade metasediments and orthogneisses showing an important contribution from Archean crust (Nd isotope and inherited zircons) and were intensively reworked during the Pan-African orogeny (Toteu et al., 2001). The Pan-African has also developed the late-Neoproterozoic Lom schist belt (Soba et al., 1991 and Toteu et al., this volume) and numerous dextral transcurrent shear zones underlined by low- to medium-grade mylonites.

The Adamawa-Yade batholith consists of a great variety of more or less deformed rock-types of different ages. Except for the sub-circular post-tectonic plutons, which have been easily mapped due to their high relief, there is a very poor cartographic distinction between the other components of the batholith; thus detailed mapping of the batholith is necessary. The various lithologies of the batholith include: dominant biotite and amphibole granites, biotite granites, biotite, amphibole and pyroxene granites, biotite and muscovite granites, diorites, gabbros, and syenites. According to the state of deformation, these rock-types have been classified as syntectonic, late-tectonic and post-tectonic (Lasserre, 1961 and Toteu et al., 2001). The few geochemical data that are available for the batholith are from the late to post-tectonic granitoids of the Lom region and show a transitional composition (Soba, 1989).

Numerous Rb–Sr whole-rock and mineral ages in the range 500–600 Ma have been recorded in the Adamawa-Yade batholith in Cameroon, Chad and Central African Republic (Bessoles and Trompette, 1980). Preliminary U–Pb zircon ages on two granitoids of the Ngaoundéré region yielded 622 ± 25 Ma for the Moungel orthogneiss and very discordant plots with upper intercept at 635 ± 22 Ma for the Ngaoundéré granite (cf. samples 83–27 and 83–38 respectively, Toteu et al., 2001); on the other hand, there are indications of ca. 800–1036 Ma inherited zircons in some granitoids of the same region (Toteu et al., 2001). Nd crustal residence ages from the northern border of the batholith at Makat are between 1.16 and 1.94 Ga with ε_{Nd} at 600 Ma from −0.8 to −9.2. One sample of medium-grained biotite–muscovite granite west of Moungel yielded an age of 1.09 Ga with ε_{Nd} at 600 Ma of −1.5 (Toteu et al., 2001). The choice of the Ngaoundéré region for the beginning of the study of the Adamawa-Yade batholith was justified by the presence of these preliminary isotopic data.

The host rocks of the Adamawa-Yade batholith in the Ngaoundéré region crop out north of Ngaoundéré and comprise alternating layers of more or less migmatized hornblende–biotite- and biotite–garnet gneisses, associated with mafic to intermediate orthogneisses and amphibolites (Fig. 2). The dominant structural feature of these rocks is the presence of a steep NE–SW mylonitic foliation associated with the regional-scale sinistral Tchollire-Banyo shear zone. This shear zone is the latest stage of a polyphase D_1–D_2 deformation associated with a high-grade Pan-African metamorphism that overprinted Palaeoproterozoic relicts of granulitic assemblages (Penaye et al., 1989). The region was subsequently affected by WSW–ENE dextral faults of the CCSZ. Granitoids of the Ngaoundéré region can be grouped into pre-tectonic granitoids represented by the hornblende–biotite granitoids (HBG), syn- to late-tectonic granitoids represented by the biotite ± mucovite granitoids (BMG), and post-tectonic granitoids represented by the porphyritic biotite ± hornblende granitoids (BG).

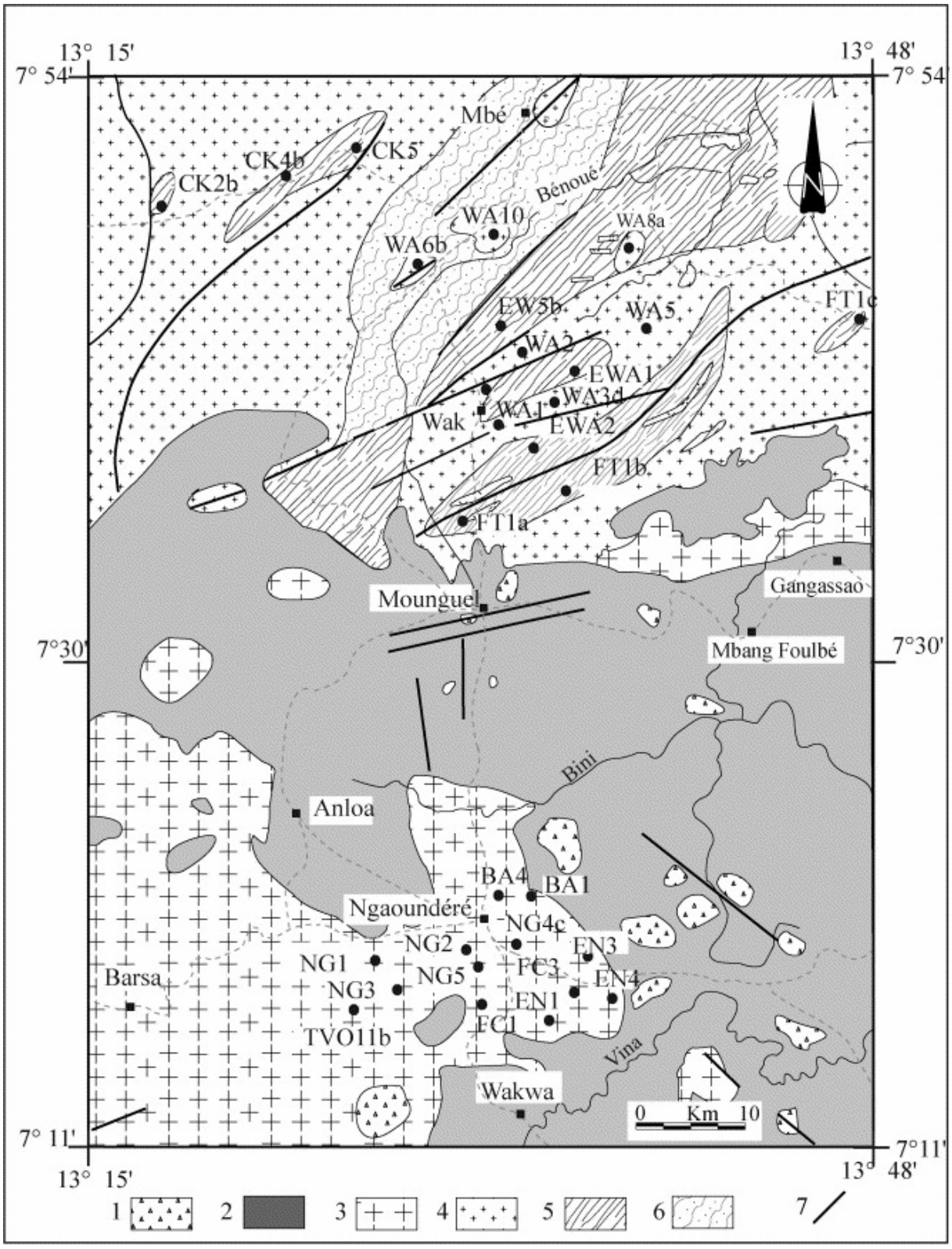

Fig. 2. Main geological units of the Ngaoundéré granitoids and surrounding areas (Koch, 1953, Guiraudie, 1955 and Lasserre, 1961) showing location of samples. Tertiary volcanic rocks: (1) trachyte and phonolite domes; (2) basalts. Neoproterozoic granitoids: (3) biotite ± hornblende porphyroid granitoids (BGs); (4) biotite ± muscovite granitoids; (5) hornblende biotite granitoids. Paleoproterozoic basement: (6) amphibole- and garnet gneisses; (7) faults.

3. Petrography of the Ngaoundéré Pan-African granitoids

A total of 125 rock samples from the granitoids and enclaves were collected for petrographic studies. Mineral compositions were determined using a Cameca SX-50 electron microprobe at the CNRS-University-BRGM laboratory of Orléans (France).

3.1. Pre-tectonic granitoids (HBG)

The HBG crop out as elongated massifs in the northern part of the Ngaoundéré region (Fig. 2). They are strongly deformed and transformed into orthogneisses under amphibolite facies conditions and underwent both D_1 and D_2 regional deformations. The first one is marked by a gently dipping S_1 foliation defined by elongated amphibole, biotite and plagioclase, sometimes associated with compositional banding marked by alternating dark and light layers. S_1 is subsequently transposed by P_2 upright folds with nearly horizontal fold axes. The D_2 deformation continues with development of NE–SW C_2 sinistral shear zones concordant to S_2 and associated with nearly horizontal plunging lineations. S_2 Foliation trends vary from N55°E to N70°E and dip steeply (>70°) SE or NW. D_2 is accompanied by a progressive migmatization which outlasted D_2 deformation. Several N110°E dextral shear zones occupied by felsic dykes are also present.

The HBG are pinkish grey, medium-grained and contain plagioclase ($An_{13–29}$), orthoclase, quartz, hornblende (Mg ratio = 0.31–0.50), and biotite (Mg ratio 0.36–0.41; TiO_2 1.41–3.37 wt%). Biotite occurs locally as a replacement of hornblende. Among the accessory minerals, titanite may reach 5–10 vol% in the dark layers. Other accessory minerals are magnetite, zircon, rutile and thorite. Thorite is included in rutile and magnetite. Some euhedral thorite crystals were also observed in quartz. Secondary minerals are sericite, epidote and chlorite.

3.2. Syn- to late-tectonic granitoids (BMG)

The BMG crop out as elongated intrusions into the HBG and the remobilised basement. They probably represent the margin of the Leunda massif, a very large massif that crops out north of the study area. Field evidence around Wak village shows that BMG post-dated the HBG and were emplaced during D_2 and its subsequent development. This sequence is supported by the presence of numerous enclaves of HBG progressively digested within the BMG and by the presence of ghost structures. The emplacement of BMG began during D_2 (dykes along P_2 axial plane) and continued later (cross-cutting relations). The later pulses only display a magmatic layering, including schlieren and planar organization of K-feldspars. The BMG are fine- to medium-grained with local porphyritic texture. Mineralogy consists of plagioclase ($An_{13–27}$), K-feldspar (orthoclase and microcline), quartz (or myrmekite), biotite (Mg ratio 0.32–0.51; TiO_2 2.59–3.21); muscovite (Na and Ti rich) is present in some differentiated rock types as small euhedral inclusions in feldspars or as well-shaped flakes. Accessory minerals are represented by apatite, zircon, allanite, monazite, ilmenite, and magnetite.

3.3. Post-tectonic granitoids (BG)

The post-tectonic granitoids consist of numerous sub-circular bodies which constitute hillocks in and around Ngaoundéré town (Fig. 2). It was not possible to observe the relationship with HBG and BMG because of the Cainozoic basaltic cover. Two rock types are distinguished:

dominant biotite granite and hornblende–biotite monzogranite are both characterized by equant porphyritic texture with megacrysts of K-feldspars. Microgranular mafic magmatic enclaves are locally observed.

The mineralogy of the dominant biotite granite is quite uniform and comprises potassic feldspar (orthoclase and microcline), plagioclase ($An_{2–16}$), quartz and biotite (Mg ratio 0.19–0.35; TiO_2 1.98–3.83). The scarce accessory minerals include zircon, monazite, magnetite, ilmenite, apatite, xenotime, and fluorite. Biotite occurs as dark brown or greenish yellowish flakes. Most biotite has been altered to chlorite, or broken down to epidote, magnetite, titanite and quartz. Apatite is the most common accessory mineral, occurring in various sizes from large anhedral to small hexagonal crystals as inclusions in biotite, along with magnetite. Similarly, prismatic to rounded zircon crystals are also present and some show oscillatory zoning. Monazites are anhedral to euhedral and are rich in Th (62,874 ppm in average). Xenotime occurs as small anhedral and rarely as large subhedral grains close to monazite. In some samples (NG1 and FC1) secondary muscovite occurs as small flakes of various dimensions. Myrmekites are observed as small spots disseminated in some plagioclases or invading K-feldspar and plagioclase from their margins.

The hornblende–biotite monzogranite differs from the biotite granite by the abundance of sphene and magnetite growing into hornblende (Mg ratio = 0.70–0.94). The plagioclase in the monzogranites is oligoclase ($An_{15–18}$), and biotites are rich in Mg (Mg ratio 0.47–0.70; TiO_2 2.57–3.43). The accessory minerals are zircon, magnetite, apatite and sphene.

The mafic enclaves exhibit a rounded shape and igneous texture, and they are usually surrounded by a chilled margin of variable thickness. They are fine-grained and darker than the BG hosts. These enclaves contain the same minerals as the hosting granitoid but in totally different proportions. They are broadly composed of biotite (from 40% to 50%), altered plagioclase, orthoclase and quartz.

4. Geochemical characterization

Samples weighing 0.5–1.5 kg were reduced and finely chipped. Sample chips were cleaned, crushed in an agate mortar, split by quartering and finely ground. Representative samples were analysed by ICP-AES and ICP-MS at the Centre de Recherches Pétrographiques et Géochimiques of Nancy, France.

4.1. Classification of the granitoids

Major and trace element data for representative samples of granitoids are listed in Table 1. We used the normative ANOR vs Q' diagram (Fig. 3) of Streckeisen and Le Maitre (1979) for nomenclature. HBG evolve from diorite, monzodiorite, quartz monzodiorite to granodiorite fields. BMG and BG have a syenogranitic composition. The sample BA-4, corresponding to a porphyritic biotite hornblende monzogranitic facies of BG, plots in the quartz syenite field. Based on the Al saturation index (A/CNK = molar $Al_2O_3/(CaO + Na_2O + K_2O)$) of Shand (1927), HBG are metaluminous, while BG and BMG are metaluminous to slightly peraluminous. In the A/CNK vs SiO_2 diagram (Fig. 4), only the most evolved BMG sample overlaps the S-type granite field; all the other rocks are in the I-type granite field. I-type geochemical signature of HBG is supported by the mineralogy (predominance of hornblende, biotite as mafic silicate minerals, and the abundance of sphene and magnetite as accessory phases). In the AFM and $(Na_2O + K_2O)$ vs SiO_2 diagrams (not shown) granitoids show a calc-

alkaline trend and plot mostly in the field of high-K calc-alkaline series (Pecerillo and Taylor, 1976; Fig. 5).

Table 1. : Representative analyses of Ngaoundéré granitoids. Analyses performed by ICP-AES and ICP-MS at the Centre de Recherches Pétrographiques et Géochimiques (CRPG) of Nancy, France

	Biotite–muscovite granitoids							Biotite Granitoids										Hornblende biotite granitoids									
	WA-5	WA-3D	WA-2	WA1	WA-10	WA 8A	WA6b	BA-4	NG4c	BA1	FC-1	FC-3	NG-1	EN1	EN4	TVO-11b	EN-3	EWA-2	CK-2b	CK5	EWA-5b	EWA1	FT1c	FT-1a	CK-4b	FT-1b
Major elements (wt%)																											
SiO_2	68.98	69.78	70.18	70.21	72.18	72.5	74.46	65.21	66.12	71.49	71.84	72.22	72.23	73.13	73.71	73.84	73.93	50.11	50.93	52.33	54.94	56.73	59.68	60.49	68.18	69.44
Al_2O_3	14.68	14.76	14.71	15.41	14.68	16.1	13.90	15.34	14.69	14.69	13.96	13.71	14.34	13.40	13.60	14.12	13.01	17.9	17.66	22.36	17.53	15.15	16.97	17.10	15.47	15.47
TiO_2	0.46	0.45	0.43	0.38	0.2	0.06	0.12	0.74	0.92	0.25	0.25	0.30	0.21	0.30	0.22	0.19	0.28	1.76	1.39	0.91	1.02	2.03	0.86	0.84	0.49	0.38
Fe_2O_3t	2.93	2.76	2.54	2.50	1.59	0.7	1.23	4.17	7.13	3.03	2.23	2.31	1.94	2.56	1.93	1.90	2.68	10.54	9.65	6.07	8.04	8.73	6.68	6.00	3.57	2.78
MnO	<L.D.	<L.D.	0.05	0.03	<L.D.	0.04	<L.D.	0.07	0.15	0.04	0.03	0.03	<L.D.	0.05	0.03	<L.D.	0.04	0.18	0.12	0.07	0.12	0.10	0.11	0.09	0.04	<L.D.
MgO	0.63	0.52	0.75	0.51	0.36	0.05	<L.D.	1.78	1.23	<L.D.	0.4	0.34	0.12	<L.D.	<L.D.	0.16	0.44	4.17	5.46	2.47	4.12	3.22	2.90	2.49	1.39	1.09
CaO	1.30	1.43	1.17	1.79	1.69	0.77	0.69	2.55	1.09	0.85	0.86	1.05	0.99	1.05	0.81	0.92	0.95	8.51	6.81	8.56	6.38	4.65	5.20	4.88	2.76	3.02
Na_2O	2.50	2.7	3.37	3.62	3.18	4.65	3.06	3.73	3.95	3.71	3.45	3.86	3.71	3.51	3.28	3.19	3.48	3.78	4.09	5.05	4.30	3.11	3.91	3.86	4.28	3.57
K_2O	6.63	6.77	5.93	4.89	5.59	4.61	5.65	5.59	3.24	5.84	6.23	5.25	5.75	4.85	5.57	5.47	4.45	2.22	2.67	1.36	2.44	3.56	3.11	3.55	3.12	3.64
P_2O_5	0.16	0.15	0.15	0.14	0.11	0.01	0.04	0.43	0.26	0.10	0.1	0.05	<L.D.	0.13	0.06	<L.D.	0.08	0.33	0.47	0.31	0.38	0.94	0.37	0.31	0.19	0.11
PF	0.79	0.54	0.58	0.44	0.46	0.67	0.68	0.58	1.15	0.36	0.49	0.70	0.48	0.68	0.51	0.33	0.48	0.99	0.79	0.63	0.69	0.59	0.70	0.59	0.43	0.53
Total	99.06	99.86	99.86	99.92	100	100.7	99.83	100.2	99.93	100.4	99.84	99.82	99.77	99.66	99.72	100.1	99.82	100.49	100.04	100.1	99.96	98.81	100.5	100.20	99.92	100.03
(*A*/CNK) mol	1.08	1.03	1.04	1.06	1.02	1.14	1.12	0.91	1.23	1.05	1.00	0.98	1.02	1.04	1.05	1.10	1.06	0.74	0.80	0.88	0.82	0.87	0.88	0.90	1.00	1.01
Mg#	19.29	17.31	24.71	18.48	20.10	7.35		32.18	16.09		16.62	14.06	6.43			8.56	15.43	30.54	38.61	31.14	36.29	29.08	32.55	31.56	30.20	30.35
$T_{Monazite}$ (°C)	*944*	*977*	*943*	*869*	*879*		*830*	*829*	*991*	*939*	*842*	*873*	*859*	*939*	*898*	*861*	*901*										
T_{Zircon} (°C)	*847*	*842*	*843*	*846*	*844*	*856*	*859*	*816*	*857*	*846*	*841*	*840*	*844*	*849*	*851*	*855*	*852*									
Norme ICPW																										
ANOR	12.33	13.44	12.32	21.80	18.98	12.13	8.72	20.66	16.84	9.51	9.08	12.85	12.63	13.43	10.02	12.37	13.89	65.87	58.17	81.03	59.66	44.49	51.57	47.32	40.55	39.99
Q'	28.13	26.38	26.46	27.14	29.55	26.77	34.65	15.64	29.65	26.13	26.91	28.39	27.22	33.12	32.43	33.43	36.21	0.00	0.00	0.00	0.00	12.09	9.90	10.69	24.95	28.08
(*A*/NK) mol	1.30	1.25	1.23	1.37	1.30	1.27	1.25	1.26	1.47	1.18	1.12	1.14	1.16	1.22	1.19	1.26	1.23	2.08	1.84	2.29	1.80	1.69	1.73	1.68	1.48	1.58
Quartz	26.87	25.48	25.34	25.36	28.88	25.88	33.44	13.68	24.23	24.65	26.31	27.83	26.90	31.49	31.18	32.64	35.04	–	–	–	–	9.06	7.87	8.76	22.52	25.97
Orthose	40.85	41.20	36.04	29.11	33.61	27.41	33.71	33.28	19.50	34.59	37.74	31.90	34.77	29.02	33.23	32.90	27.06	13.31	16.04	8.12	14.63	21.59	18.53	21.17	18.59	21.67
Albite	22.06	23.53	29.33	30.85	27.37	39.59	26.14	31.80	34.04	31.47	29.92	33.58	32.12	30.07	28.02	27.47	30.30	28.16	30.56	37.61	36.92	27.00	33.35	32.97	36.51	30.43
Anorthite	5.74	6.40	5.06	8.12	7.87	3.78	3.22	8.67	3.95	3.64	3.77	4.70	5.03	4.50	3.70	4.64	4.37	25.68	22.30	34.69	21.64	17.30	19.73	19.02	12.68	14.44
Corindon	1.43	0.73	0.97	1.22	0.57	2.07	1.60	0.00	3.32	0.94	0.20	0.00	0.22	0.76	0.84	1.30	0.94	–	0.00	–	–	0.00	–	–	0.45	0.41
Ab/An	3.84	3.68	5.79	3.80	3.48	10.46	8.12	3.67	8.62	8.65	7.94	7.14	6.39	6.68	7.57	5.91	6.94	1.10	1.37	1.08	1.71	1.56	1.69	1.73	2.88	2.11
Trace elements (ppm)																										
Ba	788	705	576	968	1962		511	1767	177	366	414.2	413	357	298	322	705	266	298	1329	784	784	1097	1483	2033	786	2128
Be	1.65	1.91	2.81	2.71	2.46		2.71	4.29	11.11	3.77	5.553	6.73	9.078	8.60	8.29	2.73	7.98	2.81	1.82	1.25	3.14	2.86	3.13	2.43	1.445	1.48
Co	3.79	3.52	3.37	3.98	2.74		1.18	9.97	7.69	2.81	2.281	2.72	1.81	2.70	2.01	2.42	2.76	38.5	32.7	21.5	23.6	20.7	17.6	15.5	9.96	6.69
Cr	14.27	8.57	12.2	9.04	7.65		<L.D.	48.7	14.4	<L.D.	6.10	10.9	7.98	5.35	8.23	12.8	12.3	115	170	59.1	62.0	64.2	26.1	35.73	30.12	11.2
Cs	1.02	0.90	2.41	2.42	0.579		1.35	3.56	16.73	3.80	3.454	2.85	6.08	8.04	6.13	1.24	6.97	1.68	1.73	1.00	2.08	4.27	4.32	3.39	2.24	2.57
Cu	7.35	9.92	4.32	11.1	21.1		<L.D.	17.99	<L.D.	<L.D.	5.768	4.29	6.74	<L.D.	<L.D.	8.07	6.83	8.80	28.9	102	14.3	13.1	52.7	61.3	24.7	23.6
Ga	26.7	26.7	27.8	23.7	20.0		20.4	23.1	40.4	26.1	24.8	26.7	25.2	29.2	25.6	21.9	26.7	23.6	23.2	23.8	25.9	28.4	23.0	21.9	18.8	15.7
Ge	1.25	1.316	1.54	1.21	1.248		1.27	1.27	2.60	1.46	1.429	1.51	1.63	1.99	1.72	1.23	1.66	1.48	1.32	1.18	1.53	1.89	1.43	1.30	0.90	0.78
Hf	9.72	8.88	11.7	10.0	4.90		5.77	7.87	35.51	12.9	7.507	8.13	5.96	13.4	9.52	5.16	10.7	4.60	6.08	2.48	4.98	10.5	6.99	4.66	4.09	2.66
Nb	23.0	22.6	41.2	21.9	10.6		17.4	18.6	107	22.0	28.51	34.8	32.3	45.17	29.4	12.0	39.4	11.1	9.32	6.18	12.8	28.3	9.84	9.11	4.71	3.18
Ni	7.59	5.53	6.36	<L.D.	5.92		<L.D.	22.13	6.45	<L.D.	5.371	<L.D.	5.36	<L.D.	<L.D.	7.65	7.39	70.7	80.4	41.7	39.4	24.3	18.0	21.0	26.5	9.6
Pb	32.4	32.6	36.1	26.5	33.7		37.7	32.0	36.0	34.8	35.9	35.2	40.7	44.2	44.3	24.8	36.4	14.6	14.6	11.6	15.1	17.0	22.2	23.3	13.0	23.7
Rb	309	313	346	233	96.0		276	196	418	232	301	296	332	355	344	208	305	139	61.2	33.0	116	204	98.9	94.5	66.2	82.4
Sn	5.30	5.54	10.2	6.39	1.09		3.60	2.98	32.1	2.84	6.716	7.81	8.31	14.65	9.41	3.75	12.2	2.38	2.48	1.63	4.67	4.93	2.68	2.23	1.02	0.88
Sr	168	149	125	280	753		129	816	59.0	123	110.4	120	104	89.0	89.5	353	83.3	734	937	869	741	695	660	742	534	680
Ta	0.87	1.01	1.91	1.35	1.34		1.79	1.83	11.32	1.63	3.238	4.11	3.54	5.87	3.84	1.38	4.50	1.13	0.66	0.43	0.76	1.83	0.66	0.68	0.38	0.15
Th	79.0	83.5	79.8	46.3	41.4		33.1	30.7	215	37.0	42.07	52.9	42.6	92.4	58.2	15.0	70.4	2.22	2.45	1.95	2.19	13.15	4.92	3.01	4.30	1.52
U	2.43	2.526	6.14	5.96	2.82		5.76	5.92	25.48	4.78	7.661	8.50	7.0	14.8	12.3	1.8	15.6	1.43	0.47	1.10	1.47	3.10	2.12	1.17	1.25	0.47
V	18.4	17.3	16.4	23.0	9.84		11.3	58.7	38.1	10.3	11.75	14.0	10.0	13.5	11.2	14.1	13.9	228	196	101	162	112	131	121	49.6	46.7
Y	12.3	13.4	20.6	15.0	10.19		13.9	27.5	215.8	31.8	31.41	54.9	28.1	47.7	52.8	16.4	49.4	27.7	27.7	17.8	22.6	28.2	28.2	22.3	11.1	5.7
Zn	89.7	95.9	80.1	67.9	23.1		22.8	67.6	254	51.9	59.34	67.7	54.3	84.7	55.9	54.6	80.5	98.6	135	59.6	116	176	86.6	70.4	44.5	40.5
Zr	367	322	418	381	163		173	321	1155	491	227.4	251	180	436	297	181	340	184	246	103	201	476	289	182	162	98.1
La	127.50	196.3	136.30	64.94	77.5		32.75	73.43	162.10	149.20	55.71	82.25	66.9	134.40	82.07	55.05	81.70	21.19	40.18	23.25	28.01	108.50	39.38	43.07	29.38	16.86
Ce	257.00	395.9	279.60	129.10	153		67.29	158.70	233.30	258.10	113	157.70	124.3	254.00	160.90	101.90	164.70	51.20	93.15	49.04	67.53	234.80	72.32	74.02	53.88	30.12

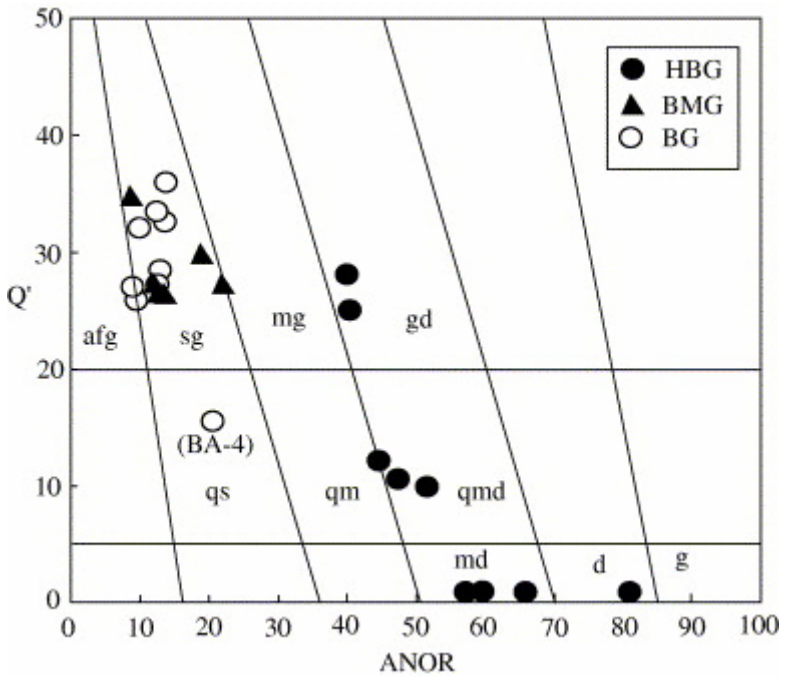

Fig. 3. Streckeisen and Le Maitre (1979) ANOR-Q' normative diagram. $Q' = 1000/(Q + Or + Ab + An)$, $ANOR = 100An/(An + Or)$. *afg*, alkali feldspar granite; *sg*, syenogranite; *mg*, monzogranite; *gd*, granodiorite; *qs*, quartz syenite; *qm*, quartz monzonite; *qmd*, quartz monzodiorite; *md*, monzodiorite; *d*, diorite; *g*, gabbro.

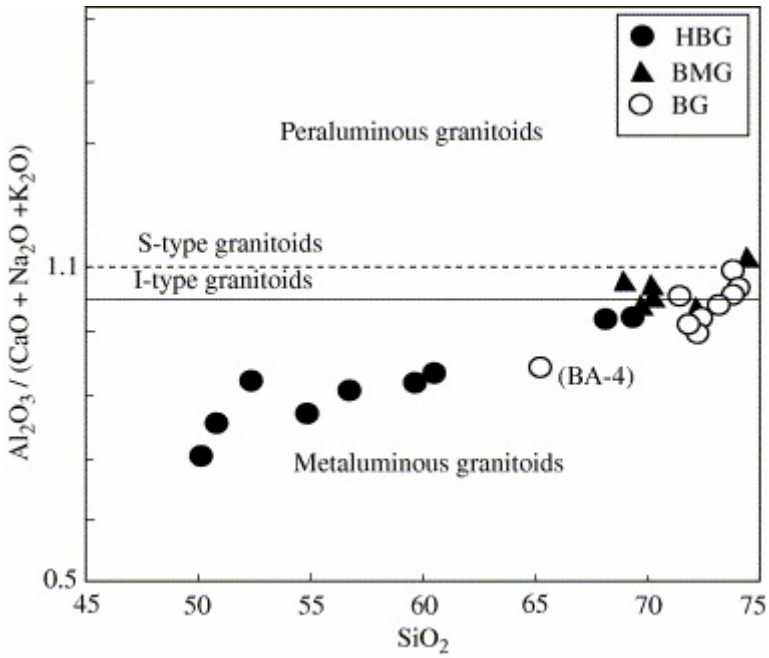

Fig. 4. Classification of the Neoproterozoic Ngaoundéré granitoids in the molar ratio $Al_2O_3/(CaO + Na_2O + K_2O)$ vs SiO_2 diagram. The subdivision between the fields of peraluminous and meta-aluminous granites is after Chappell and White (1974) while the fields of I (igneous origin) and S (sedimentary origin) granitoids are after White and Chappell (1977).

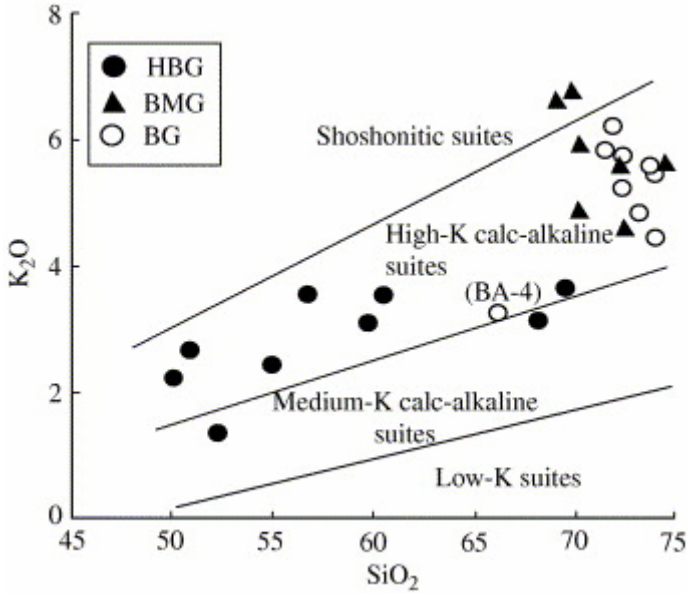

Fig. 5. K_2O vs SiO_2 diagram (Pecerillo and Taylor, 1976) for the three groups of the Neoproterozoic Ngaoundéré granitoids.

4.2. Geochemical features

4.2.1. Pre-tectonic granitoids

The HBG show an intermediate to slightly acid composition (SiO_2 = 50.1–69.4%) coupled with high Al_2O_3 (15.5–22.4 wt%) and P_2O_5 (mostly > 0.30 wt %) contents, high Mg values (Mg# = 29.1–38.6) and low K_2O/Na_2O ratios (0.3–1.1, mostly <1). Compared to other Ngaoundéré granitoids, the HBG have low abundance of Rb (33–204 ppm), Th (1.5–4.9 ppm;

except the sample EWA1 with high Th concentration, 13.1 ppm) and Zr (98–289 ppm; except the sample EWA1 with high Zr concentration, 476 ppm) and high abundance of Ba (784–2033 ppm, except the sample EWA2 with low Ba, 298 ppm), and of Sr (534–937 ppm). The Rb/Sr ratios cluster around 0.04–0.24. Chondrite-normalized REE patterns (Fig. 6A) are moderately fractionated (La_N/Yb_N 5.9–22.2, except EWA1 with La_N/Yb_N = 39.8). There are no Eu anomalies (Eu/Eu^* 0.8–1.0), but one diorite (CK5) and one granodiorite (FT1b) display a weak positive Eu anomaly (Eu/Eu^* = 1.5 and 1.4). The lack of prominent Eu anomalies and the high Sr contents exclude important fractional crystallization of feldspar in the HBG petrogenetic evolution (except for EWA1) or abundant feldspar in the residuum of the HBG source. The primitive mantle-normalized incompatible element patterns (Fig. 7A) show enrichment in LILE relative to HFSE. They are moderately fractionated with uniform negative anomalies in Nb–Ta (Nb_N/La_N = 0.1–0.5), Ti (Ti_N/Gd_N = 0.5–0.9). Samples CK5 and FT1b show positive Sr anomalies, which may be due to weak plagioclase accumulation, while EWA1, the most enriched rock (e.g., P_2O_5 = 0.94 wt%) displays a negative Sr anomaly, probably due to plagioclase and/or apatite fractionation. The very slight Ti troughs, and lower Y, Yb, and Nb values, result in a trace element distribution pattern that is characteristic of calc-alkaline arc granitoids.

4.2.2. Syn- to late-tectonic granitoids

The BMG are acid (SiO_2 = 68.9–74.5 wt%) and highly potassic (K_2O = 4.6–6.8% with $K_2O/Na_2O > 1$). They are characterized by low Sr contents (125–279 ppm), moderate Ba contents (511–968 ppm) and high abundance of Th (33.1–83.8 ppm), Rb (233–346 ppm), Zr (163–418 ppm) and REEs (∑REE = 149–822 ppm). Rb/Sr ratios range from 0.8 to 2.8. Chondrite-normalized REE patterns (Fig. 6B) show LREE enrichment with respect to HREE (La_N/Yb_N = 73–168) and strong negative Eu anomalies (Eu/Eu^* = 0.2–0.5). Compared to other Ngaoundéré granitoids they are significantly depleted and fractionated in HREE (Gd_N/Yb_N = 2.1–9.2). In the primitive mantle-normalized incompatible element diagram (Fig. 7B), all of the BMG samples display patterns with negative anomalies of Nb–Ta (Nb_N/La_N = 0.2–0.5), Sr (Sr_N/Nd_N = 0.1–0.4) (except for WA10) and Ti (Ti_N/Gd_N = 0.1–0.3). The Eu and Sr negative anomalies can be explained by plagioclase fractionation. But, the Nb, Ta and some Ti negative anomalies are inherited from the petrogenetic process.

4.2.3. Post-tectonic biotite granitoids

The biotite syenogranites are highly acid (SiO_2 = 71.5–73.9 wt%) and rich in potassium (K_2O = 4.5–6.2%) with $K_2O/Na_2O > 1$. They are characterized by low Ba (266–414, except for one sample, TVO11b with 705 ppm), low Sr (83–353 ppm), high Th (14.9–92.4 ppm, with 51.3 in average), Y (16.4–54.9 ppm), REE (∑REE = 219–556 ppm) and Rb/Sr ratios (1.9–7.1). Chondrite-normalized REE patterns (Fig. 6C) are moderately fractionated (La_N/Yb_N = 11–37, mostly <20), and show a clear Eu negative anomalies (Eu/Eu^* = 0.2–0.5) and a flat HREE profile (Gd_N/Yb_N = 1.5–2.2). In the Primitive mantle-normalized plot of incompatible trace elements, the rocks show homogenous composition with strong negative anomalies in Ti (Ti_N/Gd_N = 0.9–0.1), Sr (Sr_N/Nd_N = 0.1–0.7), Nb (Nb_N/La_N = 0.1–0.5) and Ba (Fig. 7C).

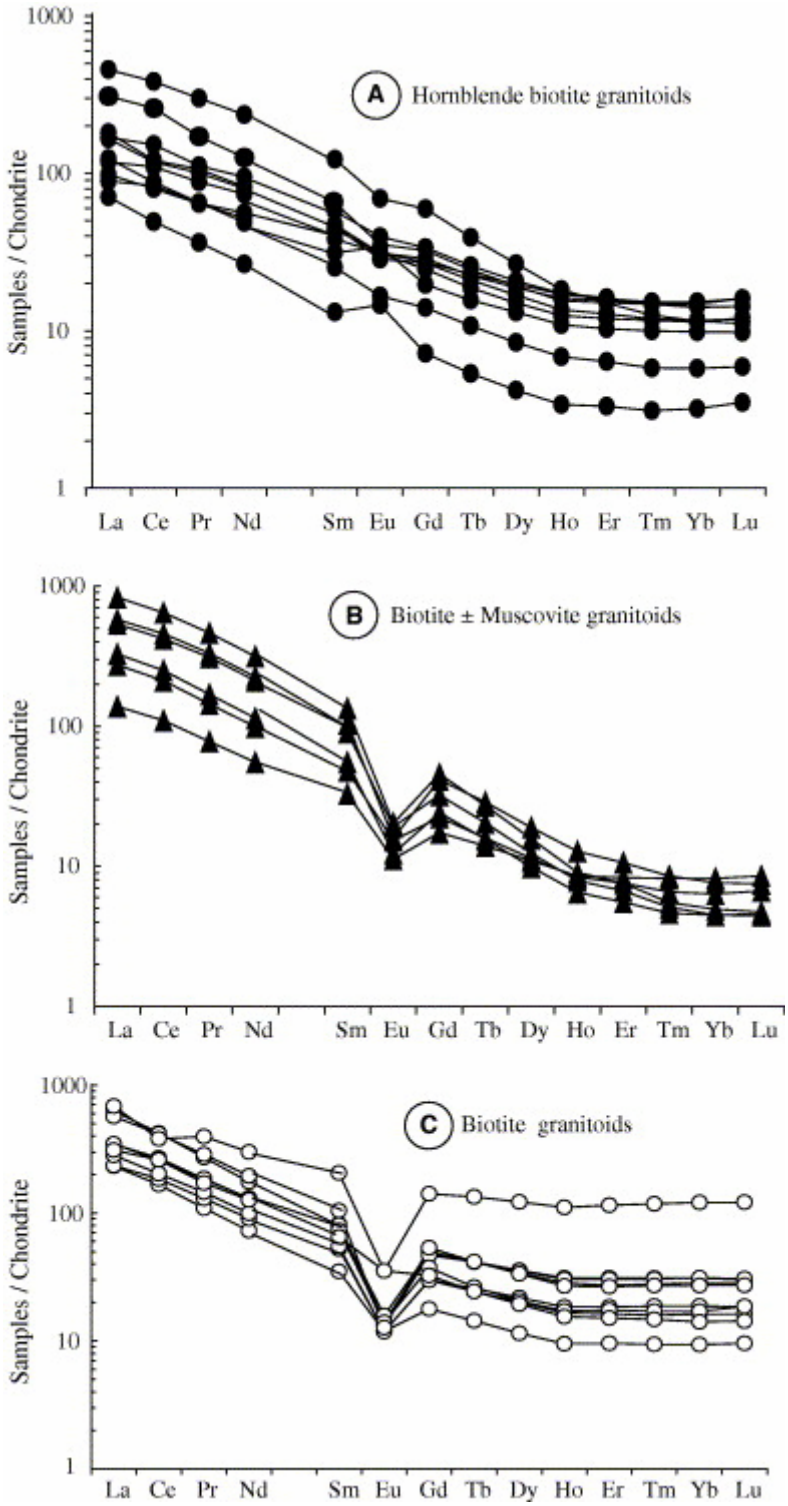

Fig. 6. Chondritic-normalized REE patterns for the Neoproterozoic Ngaoundéré granitoids. Normalizing values from Sun and McDonough (1989).

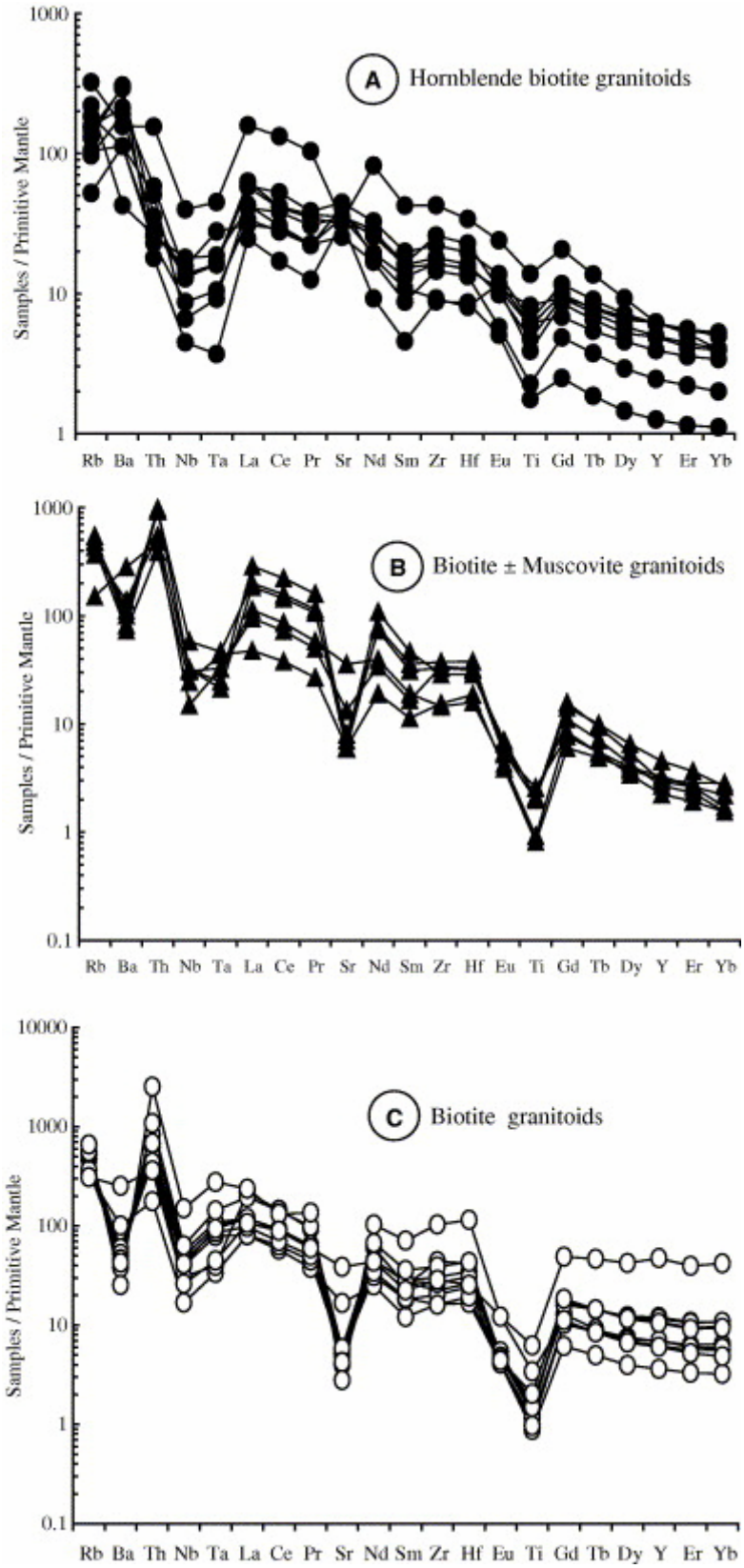

Fig. 7. Primitive mantle-normalized incompatible element patterns for the Neoproterozoic Ngaoundéré granitoids. Normalizing values from Sun and McDonough (1989).

The fine-grained mesocratic enclave (NG4c) collected in the biotite syenogranites shows higher Al_2O_3, MgO, Fe_2O_3t, TiO_2, REE, Th, Y, Rb, Nb, Hf, Zr and lower SiO_2, Sr, Ba values than all of the other biotite syenogranite samples. The REE pattern is moderately fractionated (La_N/Yb_N = 5.7), with high HREE and Y contents (Gd_N/Yb_N = 1.2 and Y = 216 ppm).

Compared to the biotite syenogranite, the porphyritic hornblende–biotite monzogranite facies of BG (sample BA-4) shows an intermediate composition (SiO_2 = 65.2 wt%). This sample displays higher Al_2O_3, Mg#, Ni, Cr, Sr, Ba and Th and lower Rb than the biotite syenogranite. The chondrite-normalized REE pattern (Fig. 6C) is moderately fractionated (La_N/Yb_N 22) with a lack of negative Eu anomalies (Eu/Eu^* = 0.8). The incompatible element pattern of the hornblende–biotite monzogranite is characterized by Nb and Ti negative anomalies and the absence of Ba and Sr anomalies (Fig. 7C).

4.3. Thermobarometry

In the ternary Q-Ab-Or normative diagram (Fig. 8A), two samples of HBG (samples with normative quartz > 10 wt%) and all the BG and BMG felsic compositions plot near or close to the water-undersaturated (a_{H2O}=0.5) granitic minimum determined experimentally to 775 °C at $P_{H_2O} - 2$ kbar by Holtz et al. (1992). The relatively high normative orthoclase content of the natural granites may be explained by pronounced H_2O-undersaturated conditions in the source materials (Scaillet et al., 1990 and Nabelek et al., 1992). Although the pressure of formation of these granites is unknown, the high orthoclase content, and therefore the generation under water-undersaturated conditions, indicates a comparatively high temperature for the melting process.

Assuming equilibrium with quartz, K-feldspar, plagioclase, titanite and magnetite, the crystallization pressure of magmatic porphyroclastic hornblende (P_{Hb}) is estimated using an experimental calibration of the Al-in-hornblende barometer (Johnson and Rutherford, 1989) and subsequent discussion (Blundy and Holland, 1990 and Schmidt, 1992). For the HBG the pressure is between 4.5 and 5.6 kbars, and for the BMG, the occurrence of primary muscovite in some differentiated samples (WA8C, WA6) places pressure limits of the crystallization at 4–2.6 kbar, i.e. the upper crust (Gardien et al., 1995 and Villa et al., 1997).

The Zr and REE contents of the melt and the mineral compositions of zircon and monazite can be used as independent chemical geothermometers for estimating the temperature of the magma (Watson and Harrison, 1983, Rapp and Watson, 1986 and Montel, 1993). We applied these thermometers to the BMG and BG to estimate the minimum temperature of the melts. The solubility model of Montel (1993) yields monazite saturation temperatures of 830–977 °C for BMG (average of 907 °C) and 842–939 °C (average of 900 °C) for BG. The zircon saturation temperatures (Watson and Harrison, 1983 and Rapp and Watson, 1986) range from 842 to 859 °C (average of 848 °C) for BMG and from 816 to 855 °C (average of 848 °C) for BG. The fine-grained mafic enclave (NG4c) exhibits higher monazite and zircon saturation temperatures (991 and 857 °C) compared to the biotite granite host rock. The monazite and zircon saturation temperatures are 777 and 738 °C respectively for the sample BA-4, the porphyritic hornblende–biotite monzogranite. The plot of the sum of LREE (La, Ce, Nd) against temperature, calculated using the monazite solubility method (Fig. 8B), shows a good positive correlation. This suggests that concentration of LREE in these rocks may be controlled by the crystallization of monazite and other accessory phases (allanite) that concentrate LREE.

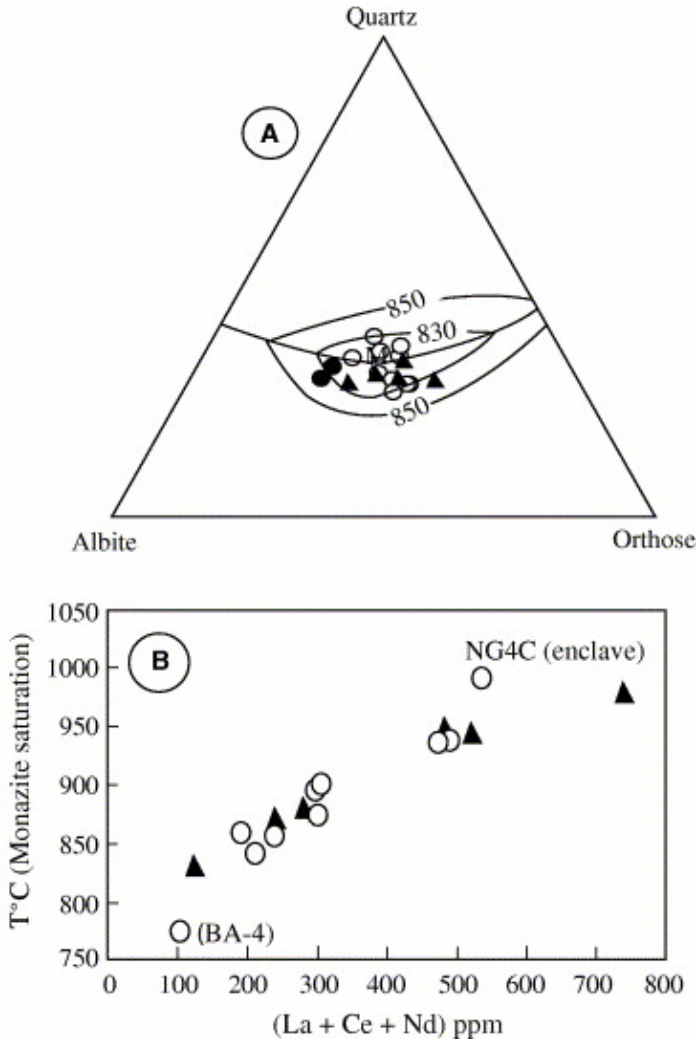

Fig. 8. (A) Composition of the Neoproterozoic Ngaoundéré granitoids plotted in the ternary normative Q-Ab-Or diagram determined experimentally by Holtz et al. (1992) (at $P_{H_2O} - 2\,kb$ and a_{H2O}=0.5). M, eutectic minimum; 830, 850, liquidus temperatures (°C). (B) (La + Ce + Nd) plotted against the *T* °C estimated from the monazite thermometry (Montel, 1993) for the Neoproterozoic BMG and BG. Symbols as in Fig. 5.

5. Chemical Th–U–Pb monazite dating

BG and BMG yielded enough monazite for chemical Th–U–Pb dating. Two samples of BG (EN-4 and NG-3) and two samples of BMG (WA3D and WA10) were collected. Analyses were carried out using a Cameca SX-100 electron probe microanalyser at the BRGM-CNRS-Université d'Orléans laboratory (France), on in situ grains (NG3, WA-3D and WA-10) and on grains mounted in resin (EN4). The analytical procedure was described by Suzuki and Adachi, 1991, Suzuki and Adachi, 1994, Montel et al., 1996, Cocherie et al., 1998 and Cocherie and Albarède, 2001. Average weighted ages calculation was performed using the Isoplot/exe program (Ludwig, 2000) and refined with Th/Pb vs U/Pb isochron plot (Cocherie and Albarède, 2001). The analytical results are given in Table 2.

Table 2. : Analytical data for monazite from biotite granitoids and biotite ± muscovite granitoids

Pr	29.49	43.96	31.50	13.69	16.09		7.39	16.34	37.49	25.80	12.35	17.35	13.78	27.25	17.64	10.38	17.54	6.15	10.64	6.09	8.42	28.52	9.57	10.08	6.203	3.447
Nd	99.02	147.2	105.60	46.24	53.31		25.74	58.93	140.00	81.79	42.36	60.96	46.49	91.02	60.84	33.91	61.11	26.22	44.17	24.30	34.58	110.50	37.32	38.42	22.75	12.43
Sm	13.85	20.56	15.99	7.35	8.433		5.04	9.93	31.43	11.18	8.015	12.03	8.367	15.94	12.30	5.36	12.48	5.84	8.80	4.79	7.08	18.80	7.21	6.77	3.873	2.011
Eu	1.11	1.175	0.93	0.89	0.717		0.65	2.05	2.05	0.81	0.685	0.91	0.686	0.74	0.76	0.69	0.81	1.81	2.30	1.98	1.65	4.02	1.81	1.80	0.964	0.848
Gd	6.61	9.396	8.51	4.59	4.968		3.58	6.67	29.02	7.69	6.149	10.25	6.12	10.96	9.63	3.65	10.08	5.59	6.94	4.05	5.53	12.26	5.90	5.05	2.882	1.478
Tb	0.77	1.013	1.07	0.60	0.585		0.53	0.91	5.01	0.98	0.96	1.55	0.917	1.56	1.55	0.54	1.54	0.86	0.97	0.58	0.78	1.47	0.84	0.70	0.403	0.2
Dy	3.15	3.977	4.80	2.90	2.505		2.78	4.91	31.03	5.22	5.526	9.03	5.1	8.50	8.96	2.92	8.65	5.03	5.26	3.34	4.28	6.78	4.79	3.82	2.142	1.062
Ho	0.45	0.511	0.73	0.47	0.368		0.48	0.88	6.26	0.97	1.045	1.76	0.939	1.52	1.72	0.54	1.60	0.97	0.98	0.62	0.77	1.03	0.91	0.71	0.387	0.192
Er	1.11	1.258	1.76	1.26	0.919		1.38	2.50	19.05	2.87	3.054	5.15	2.695	4.40	5.03	1.59	4.51	2.64	2.68	1.71	2.12	2.49	2.59	1.98	1.054	0.548
Tm	0.13	0.141	0.22	0.17	0.118		0.21	0.38	3.01	0.44	0.477	0.79	0.404	0.69	0.78	0.24	0.71	0.39	0.37	0.26	0.30	0.32	0.38	0.30	0.148	0.079
Yb	0.76	0.84	1.30	1.08	0.764		1.40	2.39	20.58	2.90	3.183	5.25	2.759	4.62	5.30	1.59	4.82	2.60	2.43	1.67	1.99	1.96	2.52	1.94	0.981	0.545
Lu	0.11	0.12	0.19	0.17	0.116		0.22	0.36	3.08	0.47	0.471	0.76	0.413	0.69	0.78	0.24	0.71	0.41	0.36	0.25	0.30	0.28	0.41	0.31	0.15	0.089
Total REE	541.05	822.35	588.49	273.45	319.39		149.44	338.37	723.40	548.43	252.99	365.75	279.87	556.29	368.24	218.59	370.95	130.87	219.22	121.92	163.34	531.73	185.93	188.96	125.20	69.91
(La/Yb)N	119.86	167.63	75.21	43.01	72.76		16.79	22.01	5.65	36.92	12.55	11.23	17.39	20.88	11.12	24.85	12.17	5.86	11.87	10.00	10.12	39.77	11.22	15.96	21.48	22.19
(Gd/Yb)N	7.16	9.25	5.42	3.51	5.38		2.12	2.31	1.17	2.19	1.60	1.61	1.84	1.96	1.50	1.90	1.73	1.78	2.36	2.01	2.30	5.18	1.94	2.16	2.43	2.24
(La/Sm)N	5.94	6.16	5.50	5.70	5.93		4.20	4.77	3.33	8.62	4.49	4.41	5.16	5.44	4.31	6.64	4.23	2.34	2.95	3.13	2.56	3.73	3.53	4.11	4.90	5.41
Eu/Eu*	0.36	0.26	0.24	0.47	0.34		0.47	0.77	0.21	0.27	0.30	0.25	0.29	0.17	0.21	0.48	0.22	0.97	0.90	1.37	0.81	0.81	0.85	0.94	0.88	1.50

Analytical errors are <5% for major elements and in the range 5–10% for trace elements and REE.

5.1. Biotite–muscovite granitoids (BMG)

Two BMG samples (WA3D and WA10) were investigated. Monazite is fresh and associated with allanite. A total of 35 chemical spot ages on three grains was obtained from sample WA3D. The calculated age histogram displays a Gaussian distribution indicating a homogeneous population. Spot ages range from 880 ± 55 to 1008 ± 65 Ma with an average weighted age of 926 ± 12 Ma (Fig. 9A), not different from the 926 ± 12 Ma obtained with the Th/Pb vs U/Pb plot. Monazites from the sample WA10 are very small in size. Its average age, calculated directly from the four individual ages is 615 ± 27 Ma (Fig. 9B). This age is very different from that obtained for sample WA3D and indicates the presence of monazites of various ages in the BMG.

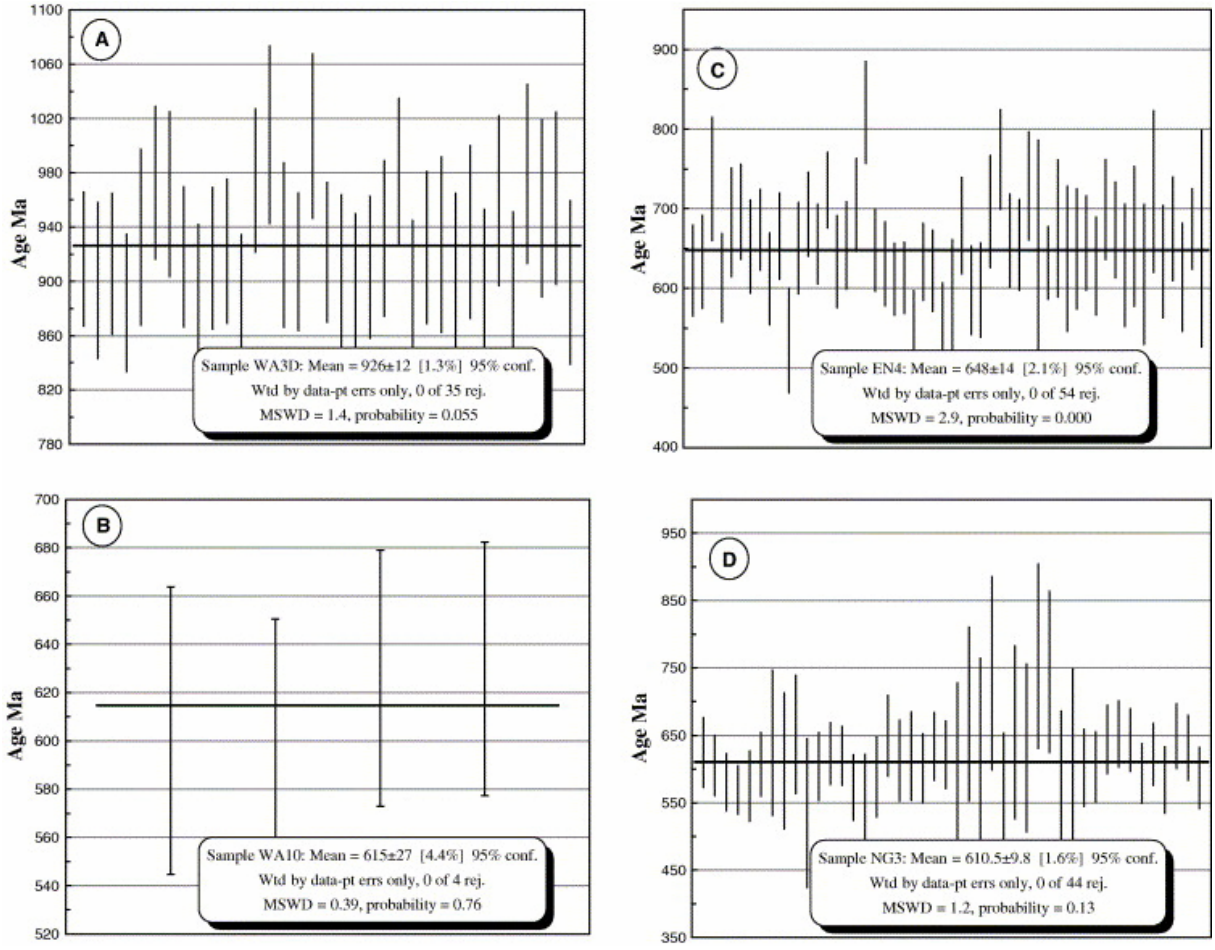

Fig. 9. Plots of average weighted age using individual ages and errors (2σ) for the monazite from biotite muscovite granitoids (A, sample WA3D; B, sample WA10) and for biotite granitoids (C, sample NG3; D, sample EN4).

5.2. Biotite granitoids (BG)

Two samples (samples NG3 and EN4) of biotite granites were investigated for monazite dating. The monazite occurs as inclusions in feldspar or biotite, where it is associated with zircon. A total of 44 chemical spot ages on four monazite grains was obtained from sample NG3, and a total of 54 spot ages on three monazite grains from sample EN4. The age histogram for monazites from each sample defines a Gaussian distribution indicating a

monogenetic population in each sample. The average weighted ages are 648 ± 14 Ma for EN4 (Fig. 9C) and 610 ± 10 Ma for NG3 (Fig. 9d) respectively. The precision of these ages using the Th/Pb vs U/Pb plot (Cocherie and Albarède, 2001) gives 652 ± 10 and 610 ± 17 Ma for EN4 and NG3 respectively.

5.3. Interpretation of the results

Field observations indicate that the HBG and BMG are respectively pre- tectonic and syn-tectonic while the BGs are post-tectonic. The zircon age of 622 ± 25 Ma obtained on the HBG, the age of younger monazites in BMG (615 ± 54 Ma), and in BGs (610 ± 10 Ma) are consistent within the error limits with the age of the syntectonic granitoids of northern Cameroon (Toteu et al., 2004). We interpreted these ages as the emplacement age of the HBG and BMG. As a consequence, the ca. 926 ± 12 Ma monazites of BMGs are inherited grains. Similarly, the 652 ± 10 Ma monazites of the post-tectonic BGs also correspond to inherited grains.

To understand the significance of the 610 ± 10 Ma monazites of BG, we recall the U–Pb results for bulk zircon analyses of the same granite (83–38, Toteu et al., 2001) which yielded very discordant ages with an upper intercept at 635 ± 22 Ma. One additional data point for a single zircon from the same sample (unpublished data from Toteu) is slightly above the concordia with a $^{206}Pb/^{238}U$ age of 575 ± 8 Ma. This suggests that the 635 ± 22 Ma intercept does not correspond to the emplacement age, but rather represents a mean age of mixed populations that include inherited and young syn-magmatic zircons. This means that the emplacement age of the Ngaoundéré biotite granite is probably close to 575 Ma, identical to the individual lower monazite spot ages. As a consequence, monazittes with the 610 ± 10 Ma ages may be interpreted as inherited grains.

Our data also give some indications of the age of the source for BMG and BG. The inherited monazites with ages of ca. 926 Ma recorded for BMG and the 1.09 Ga T_{DM} age on a similar granite west of Moungel indicate an early Neoproterozoic source for the protolith. Ages of this range are also known on detrital zircons from metasediments in Cameroon (Toteu et al., this volume) and in NE Brazil where they are related to the Cariris Velhos event (Van Schmus et al., 1995 and Santos et al., 1997).

The presence of younger inherited monazites and zircons in BG also suggests the contribution of a Neoproterozoic source to the protolith. Although country rocks for the Ngaoundéré granitoids are of Paleoproterozoic age, no indication of monazite or zircon of this age has been recorded. This is an indication that inherited monazites and zircons are probably from the source, rather than from contamination by the country rocks. In conclusion, the present study strongly suggests a major contribution of a Neoproterozoic source to the generation of the Ngaoundéré granitoids.

6. Discussion

6.1. Source rock characteristics

The Ngaoundéré granitoids display mineralogical and chemical features of I-type granites (Fig. 4) and belong to high-K calc-alkaline suites (Fig. 5). Considering the Ba and Sr abundances (Table 1), the HBG correspond to the typical high-Ba–Sr granitoids, though BG

and BMG are low-Ba–Sr granitoids (Tarney and Jones, 1994, Fowler et al., 2001 and Quian et al., 2003). Major and trace element data of the HBG high-Ba–Sr granitoids agree with differentiation of a mafic magma from an enriched subcontinental lithospheric mantle (Fig. 10), with possible crustal assimilation, as shown by the high Th/Yb and Rb/Th ratios compared to the Rb contents. The HREE undepleted patterns indicate melting of a source with a residual HREE-rich phase such as garnet.

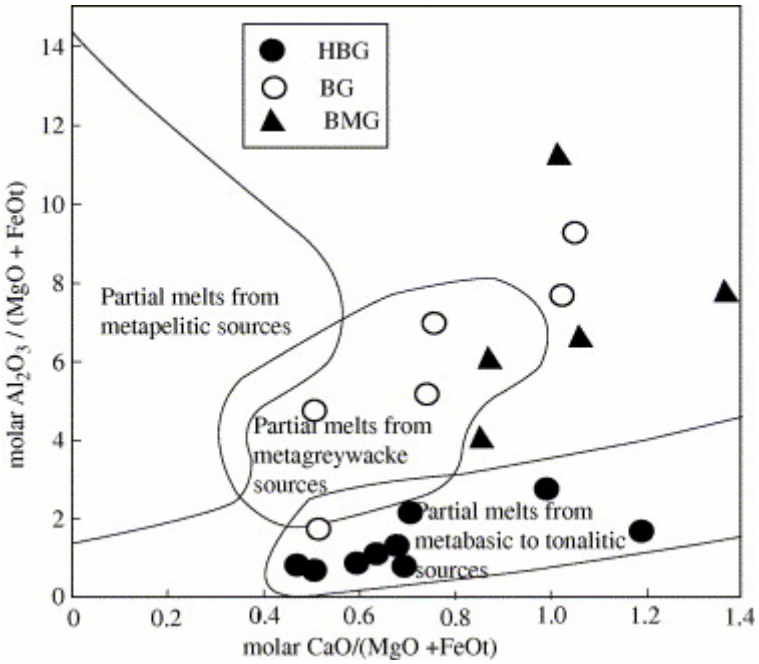

Fig. 10. Plots of the Neoproterozoic Ngaoundéré granitoids in a molar Al_2O_3/(MgO + FeOt)–CaO/(MgO + FeOt) diagram (Altherr et al., 2000), with composition fields of partial melts deriving from experimental dehydratation–melting of various source rocks (Wolf and Wyllie, 1994, Gardien et al., 1995, Partino Douce and Beard, 1995, Partino Douce and Beard, 1996 and Singh and Johanneses, 1996).

The BG and BMG trace element patterns (Fig. 7) are also characterized by strong Th- and LREE-enrichment. They may derive from partial melting of igneous protoliths (Fig. 10), but at a temperature above monazite and zircon saturation temperatures (>750 °C). The presence of inherited monazite (ca. 926 Ma), the presence of numerous enclaves of HBG progressively digested within the BMG, and the presence of ghost structures are all the consequence of a significant crustal contribution. BG that show weak Ta negative anomalies and low Nb/Ta ratios (Fig. 7) may have originated from a lower to middle crust of mafic to intermediate composition with inherited low Nb/Ta ratio (metagreywackes?) (Fig. 10), because these Nb–Ta abundances cannot be explained either by titanite–rutile fractionation or by the presence of these phases as source residue (Green and Pearson, 1987).

BMG are characterized by the presence of enclaves of HBG that occur mostly along the margin of the intrusion. This indicates that enclaves were incorporated during the emplacement and do not represent restites from the source. This is confirmed by the geochemical data (Fig. 6, Fig. 10 and Fig. 11), which indicate that BMG and HBG intrusions originated from a distinct source.

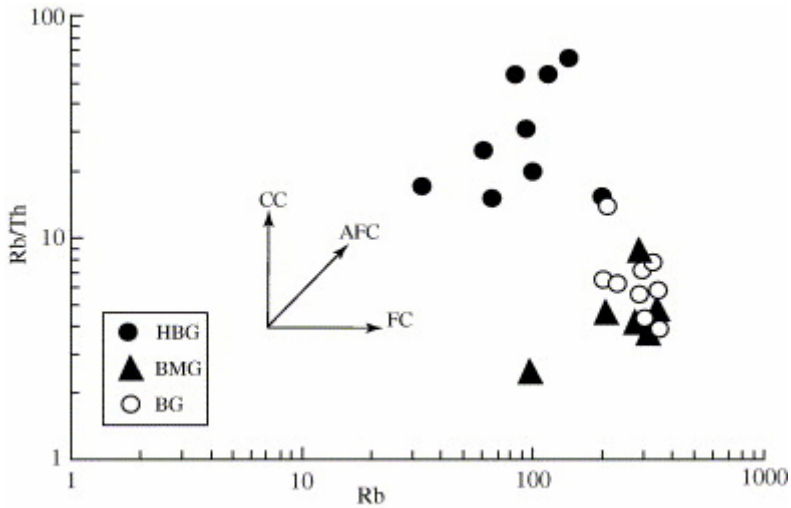

Fig. 11. Rb vs Rb/Th diagram for the Ngaoundéré Neoproterozoic granitoids. AFC, assimilation–fractional crystallization; CC, crustal contamination; FC, fractional crystallization.

6.2. Tectonic settings and tentative geodynamic context

The overall geochemical features of the Ngaoundéré granitoids are compatible with the compositions of calc-alkaline magmas of orogenic domains. In the Y + Nb vs Rb discrimination diagram (Pearce et al., 1984; Fig. 12), the HBG clearly plot within the volcanic-arc granite field, while BG plot in the within-plate granite field. The BMG plot in the field of syn-collisional granites. On the Zr vs $(Nb/Zr)_N$ diagram (Fig. 13) of Thiéblemont and Tegyey (1994), most HBG plot from the subduction to collision zone fields while BMG plot in the collision zone field, and BG overlap the collision and intra-plate fields. These characteristics and their high-potassic calc-alkaline compositions are consistent with a continental collision setting (Liégeois et al., 1994, Liégeois et al., 1998 and Toteu et al., 2004). Therefore, some within-plate granite features observed in the BG (Fig. 12) may be interpreted as an evolved trend of calc-alkaline suites, as shown by the trace element patterns (Fig. 7C). These geochemical features are similar to those documented for numerous syn- to late-collisional Pan-African granitoids of western Cameroon (Nguiessi Tchankam et al., 1997, Tagne-Kamga, 2003 and Nzolang et al., 2003). Compared to the granitoids of NE Brazil, the HBG with lower FeOt/(FeOt + MgO) ratios ($\leqslant$0.70), Nb, Y, Yb, and K_2O are similar to the normal calc-alkaline and high-K calc-alkaline granitoids (Conceiçao and Itaporanga types), whereas the BG and BMG that have higher contents of alkalis, lower contents of Ba and Sr, high FeOt/(FeOt + MgO) ratios ($\geqslant$0.70), and pronounced Eu anomalies, are similar to the calc-alkaline to transitional granitoids of Solidão and Cerra Blanca type (Guimarães et al., 1998 and Guimarães and da Silva Filho, 2000).

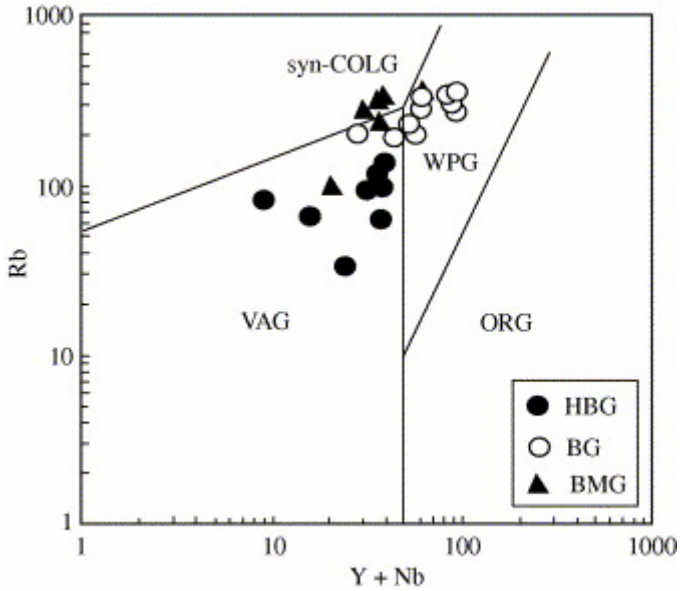

Fig. 12. (Y + Nb) vs Rb discrimination diagram for the Ngaoundéré Neoproterozoic granitoids after Pearce et al. (1984). Syn-COLG, syn-collision granite; VAG, volcanic arc granite; WPG, within-plate granite; ORG, ocean ridge granite.

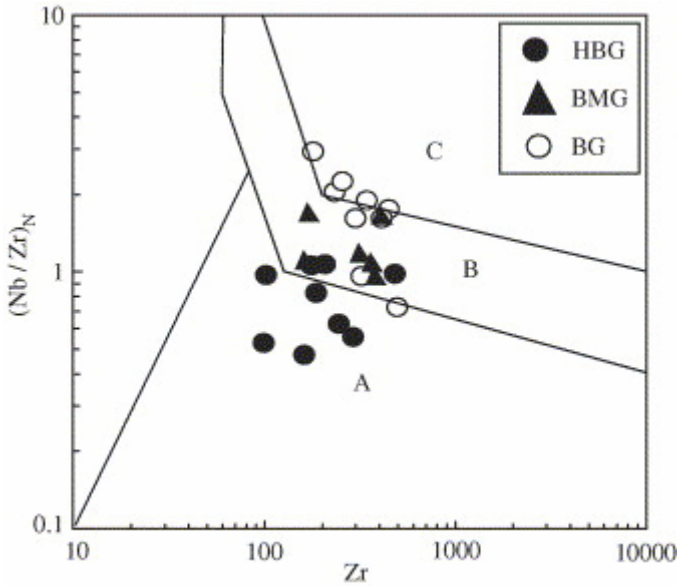

Fig. 13. Zr vs $(Nb/Zr)_N$ diagram of Thiéblemont and Tegyey (1994) for the Neoproterozoic Ngaoundéré granitoids: (A) subduction-zone magmatic rocks, (B) collision zone rocks; (C) alkaline intra-plate zone rocks. Normalization values from Sun and McDonough (1989).

A BRGM (Bureau de Recherches Géologiques et Minières d'Orléans) database, including a compilation of analyses of recent Andean lavas (Thiéblemont, 1999), was used to test further the analogy between the Ngaoundéré Neoproterozoic granitoids and Andean magmatic rocks. Averaged analyses were calculated (Table 3) using only the highly potassic calc-alkaline lavas from the central Andes. For comparison with the HBG, the Andean average was calculated in the 60% $\leqslant SiO_2 \leqslant$ 68% interval, based on $\sim$400 determinations of major elements and 100–400 determinations for trace elements, depending on the elements. For many elements (Hf, Zr, and most of the REE in particular), this average shows low standard deviations (Table 3), which makes it possible to assign a representative composition at the scale of the central Andes. The average compositions of Andean rocks and HBG show strong analogies (Fig. 14), but also show differences among some trace elements, such as Ba and Sr.

These elements show high standard deviations, however, and cannot be used for comparison with other granitoid suites.

Table 3. : Average chemical analyses for the hornblende biotite granitoids and biotite granitoids

Neoproterozoic		**Central Andes average**			**Neoproterozoic**	**Central Andes average**		
Ngaoundéré Average HBG (*n* = 9)		**Average calc-alkaline lavas SiO_2 = 60–68%**			**Ngaoundéré Average BG (*n* = 9)**	**Average calc-alkaline lavas SiO_2 > 70%**		
		Average	**Standard deviation**	***n***		**Average**	**Standard deviation**	***n***
Major elements (*wt%*)								
SiO_2	58.09	63.2	1.78	418	71.95	72.74	2.16	89
Al_2O_3	17.29	16.27	0.73	383	14.02	14.13	1.25	83
TiO_2	1.08	0.8	0.17	382	0.30	0.26	0.14	83
Fe_2O_3t	6.89	4.96	1.09	391	2.53	1.66	0.8	83
MnO	0.104	0.08	0.04	383	0.03	0.06	0.03	82
MgO	3.03	2.14	0.61	383	0.36	0.49	0.32	84
CaO	5.64	4.53	2.35	383	1.11	1.58	0.81	84
Na_2O	3.99	3.78	0.57	383	3.55	3.66	0.79	84
K_2O	2.85	3.11	0.53	413	5.44	4.31	0.97	89
P_2O_5	0.38	0.39	0.08	326	0.11	0.08	0.06	75
LOI	0.66	1.17			0.51			
Total	100.00				99.92			
Trace elements (*ppm*)								
Ba	1191	869	289	322	545	626	350	56
Co	20.73	18	9	261	3.28	9	14.4	42
Cr	63.73	37	31	262	12.48	10	9	38
Hf	5.22	5.41	0.65	148	9.01	4.07	0.84	30
Nb	10.5	12.8	6.4	167	29.12	18.4	7.9	24
Ni	36.83	16	11	290	5.32	9	21	47
Rb	99.54	109	42	377	285.26	177	95	71

Neoproterozoic		**Central Andes average**			**Neoproterozoic**	**Central Andes average**		
Ngaoundéré Average HBG (*n* = 9)		**Average calc-alkaline lavas SiO_2 = 60–68%**			**Ngaoundéré Average BG (*n* = 9)**	**Average calc-alkaline lavas SiO_2 > 70%**		
		Average	**Standard deviation**	***n***		**Average**	**Standard deviation**	***n***
Sr	732.64	558	180	399	209.85	260	190	71
Ta	0.74	1.27	0.73	127	3.33	1.67	1.55	30
Th	3.96	13.9	7.4	176	49.02	18.3	10.5	38
U	1.39	4.16	2.9	143	8.71	7.3	5.33	30
V	127.48	107	30	225	17.49	23	18.4	27
Y	21.24	17.5	5.4	160	37.77	16.4	10.3	35
Zr	215.53	195	35	241	302.66	158	68.4	49
La	38.87	39.00	9.7	184	86.74	28.2	10.1	35
Ce	80.67	80.00	22.1	149	165.92	53.3	17.9	36
Pr	9.90				17.60			
Nd	38.96	35.00	9.8	103	59.71	21.8	8.9	29
Sm	7.24	6.4	1.5	120	10.62	4.5	1.4	28
Eu	1.91	1.4	0.31	189	0.904	0.85	0.49	35
Gd	5.52	5.03	1.4	24	7.91			
Tb	0.756	0.6	0.14	179	1.167	0.4	0.15	32
Dy	4.05	3.00	0.73	11	6.53			
Ho	0.729				1.219			
Er	1.978	1.2	0.32	10	3.532			
Tm	0.283				0.544			
Yb	1.846	1.4	0.54	130	3.645	1.3	0.78	28
Lu	0.284	0.2	0.07	115	0.546	0.2	0.15	15

The average composition (and standard deviation) of the high-K calc-alkaline andesite, dacite and rhyolite from the central Andes is given for comparison (BRGM geochemical database on Andean magmatic rocks) (Thiéblemont, 1999) and was calculated using a number of measurements that varied depending on the element.

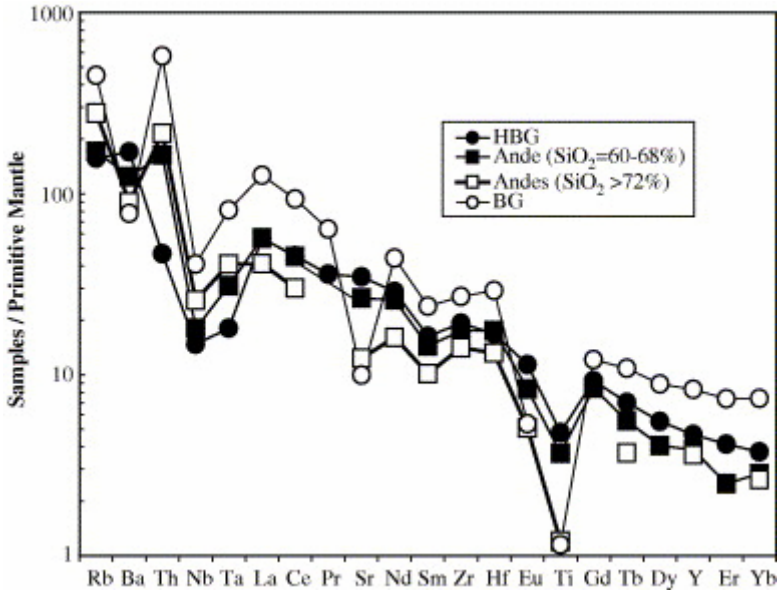

Fig. 14. Primitive mantle-normalized incompatible element patterns for the average HBGs and BGs compared to the Central Andes average of calc-alkaline lavas. Normalizing values from Sun and McDonough (1989).

For comparison with BG, the Andean average was calculated by using only the most acid rocks (i.e. $SiO_2 > 70\%$) and for an age range extending to the late Miocene. The primitive mantle-normative patterns of BG show some analogies to the Andean rocks (Fig. 14), although BG are much more differentiated. It is concluded that the Ngaoundéré granitoids in central North Cameroon that are part of the Adamawa-Yadé batholith may be the roots of a continental margin that was active during the late Neoproterozoic (Toteu et al., 2004). In pre-drift reconstructions, this active continental margin may be correlated with the Central Tectonic Domain or Transverse Zone of the Borborema province in NE Brazil (Ebert, 1970 and Van Schmus et al., 1995), which is characterized by abundant late Neoproterozoic plutonism and development of continental-scale shear zones (Neves et al., 1996).

7. Conclusions

Petrography, geochemistry and new geochronological work carried out in the Ngaoundéré region on the Adamawa-Yade batholith revealed three main types of Pan-African granitoids: the hornblende–biotite granitoids (HBG), the biotite ± muscovite granitoids (BMG), and the biotite granitoids (BG). Monazite dating is not conclusive but strongly indicates the presence of pre-magmatic monazite inheritances at ca. 926 Ma.

Geochemical data indicate that the Ngaoundéré Pan-African granitoids are calc-alkaline, high-K and of I-type. The HBG are of the high-Ba–Sr sub-type and were generated by differentiation of mafic magmas derived from an enriched subcontinental lithospheric mantle, with substantial crustal contamination. By contrast, the BGs and BMG are of a low-Ba–Sr sub-type and were possibly derived from melting of middle continental crust. Differences in these granitoid groups can be explained by variations in the source composition, the melting conditions and the degree of mineral fractionation. The large-scale melting of the source rocks could have been promoted by high heat flow during Neoproterozoic deformation and/or by the upward migration or underplating of mantle-derived magmas generated during a convergent phase.

The chemical signature of the HBG shows strong analogies with the magmatic suites of recent active margins and, more precisely, with calc-alkaline rocks of the central Andes. These analogies suggest a setting above a subduction zone at an active margin. Generation of the BMG by crustal melting may have occurred subsequent to a collisional stage, with emplacement along SW-NE left-lateral strike slip faults. Then, the BG plutons were emplaced in a post-orogenic setting.

Acknowledgements

RT thanks the Agence Universitaire de la Francophonie (AUF) for the post-doc scholarship and the Institut des Sciences de la Terre d'Orléans (ISTO) for accommodation and support of all the laboratory work. The authors are grateful to O. Rouer, G. Drouet and C.Gille for their assistance during the electron microprobe analyses. The paper benefited from critical reviews by I.P. Guimarães and D. Gasquet and from English improvement by J.J.W. Rogers. They are gratefully acknowledged. This work is a contribution to IGCP-470.

References

Altherr et al., 2000 R. Altherr, A. Holl, E. Hegner, C. Langer and H. Kreuzer, High-potassium, calc-alkaline I-type plutonism in the European Variscides: northern Vosges (France) and northern Schwarzwald (Germany), *Lithos* **50** (2000), pp. 51–73.

Bessoles and Trompette, 1980 Bessoles, B., Trompette, R., 1980. Géologie d'Afrique. La chaîne panafricaine, "zone mobile d'Afrique centrale" (partie sud) et zone soudanaise. Mémoires du B.R.G.M., Orléans N° 92, 394p.

Blundy and Holland, 1990 J.D. Blundy and T.J.B. Holland, Calcic amphibole equilibrium and a new amphibole-plagioclase geothermometer, *Contribution to Mineralogy and Petrology* **104** (1990), pp. 208–224.

Castaing et al., 1994 C. Castaing, J.-L. Feybesse, D. Thiéblement, C. Triboulet and P. Chèvremont, Paleogeographical reconstructions of the Pan-African/Brasiliano orogen: closure of an oceanic domain or intracontinental convergence between major blocks, *Precambrian Research* **69** (1994), pp. 327–344.

Chappell and White, 1974 B.W. Chappell and A.J.R. White, Two constrating granite types, *Pacific Geology* **8** (1974), pp. 173–174.

Cocherie and Albarède, 2001 A. Cocherie and F. Albarède, An improved U–Th–Pb age calculation for electron microprobe dating of monazite, *Geochimica Cosmochimica Acta* **65** (2001), pp. 4509–4522.

Cocherie et al., 1998 A. Cocherie, O. Legendre, J.J. Peucat and A.A. Kouamelan, Geochronology of polygenic monazites constrained by in situ lead behaviour in monazite, *Geochimica Cosmochimica Acta* **62** (1998), pp. 2475–2497.

Dumont, 1986 J.F. Dumont, Identification par télédétection de l'accident de la Sanaga (Cameroun), *Geodynamique* **1** (1986), pp. 13–19.

Ebert, 1970 H. Ebert, Precambrian geology of the Borborema Belt (states of Paraiba and Rio Grande do Norte, northeastern Brazil) and the origin of its mineral resources, *Geologishes Rundschau* **59** (1970), pp. 1299–1326.

Fowler et al., 2001 M.B. Fowler, P.J. Honney, D.P.F. Darbyshire and P.B. Greenwood, Petrogenesis of high-Ba–Sr granites: the Rogart pluton, Sutherland, *Journal of Geological Society Of London* **158** (2001), pp. 521–534.

Gardien et al., 1995 V. Gardien, A.B. Thompson, D. Grujic and P. Ulmer, Experimental melting of biotite + plagioclase + quartz ± muscovite assemblage and implications for crustal melting, *Journal of Geophysical Research* **100** (1995), pp. 15581–15591.

Green and Pearson, 1987 T.H. Green and N.J. Pearson, An experimental study of Nb and Ta partitioning between Ta-rich minerals and silicate liquids at high pressure and temperature, *Geochimica Cosmochimica Acta* **51** (1987), pp. 55–62.

Guimarães and da Silva Filho, 2000 I.P. Guimarães and F.A. da Silva Filho, Evidence of multiple sources involved in the genesis of the neoproterozoic itapetim granitic complex, NE Brazil, based on geochemical and isotopic data, *Journal of South America Earth Sciences* **13** (2000), pp. 561–586.

Guimarães et al., 2004 I.P. Guimarães, F.A. da Silva Filho, C.N. Almeida, W.R. Van Schmus, M.M.J. Araújo, S.C. Melo and E.B. Melo, Brasiliano (Pan-African) granitic magmatism in the Pajeú-Paraíba belt, northeast Brazil: an isotopic and geochronological approach, *Precambrian Research* **135** (2004), pp. 23–53.

Guimarães et al., 1998 Guimarães, I.P., da Silva Filho, F.A., Almeida, C.N., Araújo, M.M.J., Melee, S.C., Sales, A., 1998., The Braziliano granitoidsfro the Pajeu Paraiba Belt and Texeira High: Sm–Nd isotope geochemistry and U/Pb in zircon ages. XL Congresso Brasileiro de Geologia (Belo Horizonte, MG), Abstracts, p. 48.

Guiraudie, 1955 Guiraudie, Ch., 1955. Notice explicative sur la feuille Ngaoundéré-Ouest. Carte géologique de reconnaissance à l'échelle 1/500 000. Territoire du Cameroun, 1 carte, Paris, 23p.

Holtz et al., 1992 F. Holtz, M. Pichavant, P. Barbey and W. Johannes, Effects of H_2O liquidus phase relations in the haplogranitic system at 2 and 5 kbars, *American Mineralogist* **77** (1992), pp. 1223–1241.

Johnson and Rutherford, 1989 M.C. Johnson and M.J. Rutherford, Experimental calibration of the aluminium-in-hornblende geobarometer with application to Long Valley caldera (California) volcanic rocks, *Geology* **17** (1989), pp. 837–841.

Koch, 1953 Koch, P., 1953. Carte géologique du Cameroun au 1/500 000. Coupure Banyo, avec notice explicative. Imprimerie nationale.

Lasserre, 1961 M. Lasserre, Etude géologique de la partie orientale de l'Adamaoua (Cameroun Central) et les principales sources minéralisées de l'Adamaoua, *Bulletin de la Direction des Mines et Géologie du Cameroun* (1961) (4).

Liégeois et al., 1994 J.P. Liégeois, R. Black, J. Navez and L. Latouche, Early and late Pan-African orogenies in the Aïr assembly of terrane (Tuareg shield, Niger), *Precambrian Research* **67** (1994), pp. 59–88.

Liégeois et al., 1998 J.P. Liégeois, J. Navez, J. Hertogen and R. Black, Contrasting origin of post-collisional high-K calc-alkaline and shoshonitic versus alkaline and peralkaline granitoids. The use of sliding normalization, *Lithos* **45** (1998), pp. 1–28.

Ludwig, 2000 Ludwig, K.R., 2000. User manual for ISOPLOT/EX, version 2.4. A geohronological toolkit for Microsoft Excel. Berkeley Geochronology Center, Special Publication 1a, 53p.

Montel, 1993 J.-M. Montel, Model for monazite/melt equilibrium and application to the generation of granitic magmas, *Chemical Geology* **110** (1993), pp. 127–146.

Montel et al., 1996 J.-M. Montel, S. Foret, M. Veschambre, C. Nicollet and A. Provost, Electron microprobe dating of monazite, *Chemical Geology* **131** (1996), pp. 37–51.

Nabelek et al., 1992 P.I. Nabelek, C. Russ-Nabelek and J.R. Denison, The generation and crystallization conditions of the Proterozoic Harney Peak leucogranite, Black Hills, South Dakota, USA: petrologic and geochemical constraints, *Contributions to Mineralogy and Petrology* **110** (1992), pp. 173–191.

Neves et al., 1996 S.P. Neves, A. Vauchez and C.J. Archanjo, Shear zone controlled magma emplacement or magma-assisted nucleation of shear zones? Insights from northeast Brazil, *Tectonophysics* **26** (1996), pp. 349–365.

Neves et al., 2000 S.P. Neves, A. Vauchez and G. Feraud, Tectono-thermal evolution, magma emplacement, and shear zone development in the Caruaru area (Borborema Province, NE Brazil), *Precambrian Research* **99** (2000), pp. 1–32.

Ngako et al., 2003 V. Ngako, P. Affaton, J.M. Nnange and Th. Njanko, Pan-African tectonic evolution in central and southern Cameroon: tranpression and transtension during sinistral shear movements, *Journal of African Earth sciences* **36** (2003), pp. 207–214.

Ngako et al., 1991 V. Ngako, P. Jegouzo and J.P. Nzenti, Le Cisaillement Centre-Camerounais. Rôle structural et géodynamique dans l'orogenèse panafricaine, *Comptes rendus De l'Académie des Sciences Paris* **315** (1991), pp. 457–463.

Nguiessi Tchankam et al., 1997 C. Nguiessi Tchankam, J.P. Nzenti, E.N. Nsifa, P. Tempier and F.M. Tchoua, Les granitoïdes calco-alcalins, syn-cisaillement de Bandja dans la chaîne panafricaine nord-équatoriale au Cameroun, *Comptes Rendus De l' Académie des Sciences Paris* **325** (1997), pp. 95–101.

Nzolang et al., 2003 C. Nzolang, H. Kagami, J.P. Nzenti and F. Holtz, Geochemistry and preliminary Sr–Nd isotopic data on the Neoproterozoic granitoids from the Bantoum area, west Cameroon: evidence for a derivation from a Paleoproterozoic to Archean crust, *Polar Geosciences* **16** (2003), pp. 196–226.

Partino Douce and Beard, 1995 A.E. Partino Douce and J.S. Beard, Dehydratation–melting of biotite gneiss and quartz amphibolite from 3 to 15 kbar, *Journal of Petrology* **36** (1995), pp. 707–738.

Partino Douce and Beard, 1996 A.E. Partino Douce and J.S. Beard, Effects of P, f (O_2) and Mg/Fe ratio on dehydratation melting of model metagrreywackes, *Journal of Petrology* **37** (1996), pp. 999–1024.

Pearce et al., 1984 J.A. Pearce, N.B.W. Harris and A.G. Tiindle, Trace element discrimination diagrams for the tectonic interpretation of granitic rocks, *Journal of Petrology* **25** (1984), pp. 956–983.

Pecerillo and Taylor, 1976 A. Pecerillo and S.R. Taylor, Geochemistry of Eocene cal-alkaline volcanic rocks from the Kastamonu area, northern Turkey, *Contributions to Mineralogy and Petrology* **58** (1976), pp. 63–81.

Penaye et al., 1989 J. Penaye, S.F. Toteu, A. Michard, J.M. Bertrand and D. Dautel, Reliques granulitiques d'âge Protérozoïque inférieur dans la zone mobile panafricaine d'Afrique Centrale au Cameroun; géochronologie U/Pb sur zircons, *Comptes Rendus de l'Académie des Sciences Paris* **309** (1989), pp. 315–318.

Quian et al., 2003 Q. Quian, S.-L. Chung, T.-Y. Lee and D.-J. Wen, Mesozoic high-Ba–Sr granitoids from North China: geochemical characteristics and geological implications, *Terra Nova* **15** (2003), pp. 272–278.

Rapp and Watson, 1986 R.P. Rapp and E.B. Watson, Monazite solubility and dissolution kinetics: implication fot the thorium and light rare earth chemistry of felsic magmas, *Contributions to Mineralogy and Petrology* **94** (1986), pp. 304–316.

Santos et al., 1997 Santos, E.J., Oliveira, R.G., Paiva, I.P., 1997. Terrenos do Dominio Transversal da provincial Borborema: controles sobre acresçãe retrabalhamento crustais ao sul do lineamento Patos. In: XVII SBG symposio de Geologia do Nordeste (Fortaleza, CE), Proceedings 15, pp. 140–144.

Scaillet et al., 1990 B. Scaillet, C. France-Lannord and P. Le Fort, Badrinath-Gangotri plutons (Garhwal, India): petrological and geochemical evidence for fractionation processes in high Himalayian leucogranite, *Journal of Vocanology and Geothermal Research* **44** (1990), pp. 163–188.

Schmidt, 1992 M.W. Schmidt, Amphibole composition in tonalite as a function of pressure: an experimental calibration of the Al-in-hornblende barometer, *Contributions to Mineralogy and Petrology* **110** (1992), pp. 304–310.

Shand, 1927 S.J. Shand, Eruptive Rocks. Their Genesis, Composition, Classification, and their Relation to Ore-deposits (third ed.), J. Wiley and Sons, New York (1927) p. 488.

Singh and Johanneses, 1996 J. Singh and W. Johanneses, Dehydration melting of tonalites: Part II. Composition of melts and solids, *Contributions to Mineralogy and Petrology* **125** (1996), pp. 26–44.

Soba, 1989 Soba, D., 1989. La série du Lom: etude géologique et géochronologique d'un bassin volcanosédimentaire de la chaîne panafricaine à l'Est Cameroun. Thèse de Doctorat d'Etat, Université De Paris VI, 181p.

Soba et al., 1991 D. Soba, A. Michard, S.F. Toteu, D.I. Norman, J. Penaye, V. Ngako, J.P. Nzenti and D. Dautel, Données géochronologiques nouvelles (Rb–Sr, U–Pb et Sm–Nd) sur la zone mobile panafricaine de l'Est Cameroun: âge protérozoïque supérieur de la série de Lom, *Comptes Rendus de l'Académie des Sciences Paris* **312** (1991), pp. 1453–1458.

Streckeisen and Le Maitre, 1979 A. Streckeisen and R.W. Le Maitre, A chemical approximation to the modal QAPF classification of the igneous rocks, *Neues Jahrbuch fuer Mineralogie Abhandlung* **136** (1979), pp. 169–206.

Sun and McDonough, 1989 Sun, S.S., McDonough, W.F., 1989. Chemical and isotopic systematics of oceanic basalts: implication for mantle composition and processes. In: Saundersand, A.D., Norry, M.J. (Eds.), Magmatism in the Ocean basins Geological Society Special Publication 42, pp. 313–345.

Suzuki and Adachi, 1991 K. Suzuki and M. Adachi, The chemical Th-U-total Pb isochron ages of zircon and monazite from the grey granite of the Hida Terrane, Japan, *Journal of Earth Sciences Nagoya University* **38** (1991), pp. 11–37.

Suzuki and Adachi, 1994 K. Suzuki and M. Adachi, Middle Precambrian detrital monazite and zircon from the Hida gneiss on Oki-Dogo Island, Japan: their origin and implication for the correlation of basement gneiss of Southwest Japan and Forea, *Tectonophysics* **235** (1994), pp. 277–292.

Tagne-Kamga, 2003 G. Tagne-Kamga, Petrogenesis of the Neoproterozoic Ngondo plutonic complex (Cameroon, West central Africa): a case of late-collisional ferro-potassic magmatism, *Journal of African Earth Sciences* **36** (2003), pp. 49–171.

Tagne-Kamga et al., 1999 G. Tagne-Kamga, E. Mercier, M. Rossy and E.N. Nsifa, Synkinematic emplacement of the panafrican Ngondo igneous complex (West Cameroon, central Africa), *Journal of African Earth Sciences* **28** (1999), pp. 675–691.

Tarney and Jones, 1994 J. Tarney and C.E. Jones, Trace element geochemistry of orogenic igneous rocks and crustal growth models, *Journal of Geological Society of London* **151** (1994), pp. 855–868. Abstract-GEOBASE

Thiéblemont, 1999 D. Thiéblemont, Discrimination entre magmatismes calco-alcalins mantellique et crustal: l'exemple des Andes, *Comptes Rendus de l'Académie des Sciences Paris* **329** (1999), pp. 243–250.

Thiéblemont and Tegyey, 1994 D. Thiéblemont and M. Tegyey, Une discrimination géochimique des roches différenciées témoin de la diversité d'origine et de situation tectonique des magmas calco-alcalins, *Comptes Rendus de l'Académie des Sciences Paris* **319** (1994), pp. 87–94.

Toteu et al., 2001 S.F. Toteu, W.R. Van Schmus, J. Penaye and A. Michard, New U–Pb, and Sm–Nd data from North-Central Cameroon and its bearing on the pre-Pan-African history of Central Africa, *Precambrian Research* **108** (2001), pp. 45–73.

Toteu et al., this volume Toteu, S.F., Penaye, J., Deloule, E., Van Schmus, R.W., Tchameni, R., this volume. Diachronous evolution of volcano-sedimentary basins north of the Congo craton: insights from U–Pb ion microprobe dating of zircons from the Poli, Lom and Yaoundé Series (Cameroon). Journal of African Earth Sciences,

Toteu et al., 2004 S.F. Toteu, J. Penaye and Y. Poudjom Djomani, Geodynamic evolution of the Pan-African belt in central Africa with special reference to Cameroon, *Canadian Journal of Earth Sciences* **41** (2004), pp. 73–85.

Van Schmus et al., 1995 W.R. Van Schmus, B.B. Brito Neves, P. Harcspacher and M. Babinsky, U/Pb and Sm/Nd geochronologic studies of the eastern Borborema Province, northeastern Brazil: initial conclusions, *Journal of South American Earth Sciences* **8** (1995), pp. 267–288.

Villa et al., 1997 L.M. Villa, G. Ruggieri and M. Puxxedu, Petrological and geochronological discrimination of two-white-mica generations in a granite cored from the Larderello-Travale geothermal field (Italy), *European Journal of Mineralogy* **9** (1997), pp. 585–596.

Watson and Harrison, 1983 E.B. Watson and T.M. Harrison, Zircon saturation revisited: temperature and composition effects in a variety of crustal magma types, *Earth and Planetary Sciences Letter* **64** (1983), pp. 295–304.

White and Chappell, 1977 J.R. White and B.W. Chappell, Ultrametamorphism and granitoids genesis, *Tectonophysics* **43** (1977), pp. 7–22.

Wolf and Wyllie, 1994 M.B. Wolf and J.P. Wyllie, Dehydration–melting of amphibolite at 10 kbars: the effects of temperature and time, *Contributions to Mineralogy and Petrology* **115** (1994), pp. 369–383.